A Linear Model for Orographic Precipitation in meteorological and climatological downscaling

Giulio Nils Caroletti

Dissertation for the degree of philosophiae doctor (PhD)
at the University of Bergen

2015

Dissertation date: June 24th, 2015

Contents

Paper 4. G. Caroletti and R. Deidda: Orographic corrections of climatological precipitation downscaling combining a physical based Linear model and a Multifractal model.

Submitted to Atmospheric Research.

Abstract

Orographic precipitation has always been a major field of study in atmospheric sciences, because of its major role in the water budget and its influence on environmental hazards like floods and droughts - and thus on human activity. Understanding its features has become even more important with the rise of the challenges posed by the changing climate. In the last two decades, several models have been developed to advance orographic precipitation science.

This thesis used mainly one of these models, Smith and Barstad's Linear Model for orographic precipitation, in high space-resolution studies for downscaling and model validation, both on the meteorological and on the climatological time scales. The problem of model validation and precipitation downscaling was introduced in the first paper, while the Linear Model itself was used in downscaling in three other papers: in one instance to downscale 3- and 6-hour meteorological forecasts and reanalysis down to 250 meters of space resolution; in one case, to downscale daily climate projections of 30 years of data down to about 1 km space resolution in western Norway; and lastly, to provide orographic correction at 1 km resolution to a spatially homogeneous statistical downscaling model.

The first paper dealt with ENSEMBLES model validation at the 25 km scale. The validation was performed as part of CLIMB, an EU FP-7 project that studied climate changes at selected Mediterranean hydrological basins. The control time was 1951-2010. Model

validation allowed to select four models in the ENSEMBLES dataset for use in later stages of the project; however, it also showed that 25 km resolution was too coarse a resolution to properly resolve physical phenomena that lead to orographic precipitation, and pointed at the need for proper downscaling of precipitation and temperature data.

Starting from this, this thesis introduced the Linear Model as a tool for climatological downscaling. For climate projections, the Linear Model's low CPU demand allowed the production of many simulations to span the uncertainties over the whole model range of the projects taken into account. The four ENSEMBLES models selected in the first paper were used for the downscaling performed in Sardinia for the 1981-1990 time period in the fourth paper. In the second paper, fourteen IPCC AR4 models were used in Norway, for the 1971-2000 control period, and the 2046-2065 and 2071-2100 future assessements.

The results showed that when large-scale background precipitation is taken into account, the Linear Model was able to compare well with simulated and observational data both for Norway and for Sardinia, with promising results in i) reducing errors of past reconstruction and ii) producing reasonable climate assessments - in both instances at a high spatial resolution. The results at past control times showed that LM was able to provide a significant spatial separation of real data stations. In IPCC AR-4 downscaling in Norway, where large-scale precipitation was negligible compared to orographic precipitation, the Linear Model was able to reproduce past climatology and provide a

future assessment as a stand-alone tool. In Sardinia, the Linear Model was used in conjunction with a statistically homogeneous Multifractal model.

The use of a two-models downscaling method for Sardinia allowed to circumvent one of the Linear Model's main limitations, i.e. the fact that it is unfit for use on its own in warmer climates, where orographic forcing is just one of the components that lead to precipitation and thermal convection can play an important role. In regard to reproducing observed features of local precipitation, the Linear Model orographic correction used with the Multifractal model compared very well with a locally-calibrated orographic modulation of the same statistical model. This happened at mean areal precipitation level, but also at individual stations, for yearly means, and for monthly and daily distributions of precipitation events.

The third paper dealt with meteorological time scales, comparing three days of observations with WRF simulations, and LM downscaling of WRF data was used at different time and space resolutions over the Stord island in western Norway. In this study, the Linear Model compared well with a more complex model like WRF, in reproducing high resolution precipitation events. This was especially true at the higher spatial (250 m) and temporal (3 hours) resolutions used.

To sum up the findings of this thesis, we tested the boundaries of the Linear Model, already proven in literature to be a powerful tool for describing orographic precipitation. We showed that, with

some care, it could be used both as a stand-alone model or an accompanying support for climatological downscaling studies, and to refine or better understand investigations on precipitation carried out through meteorological methods. Good results in the use of the Linear Model for climatological studies in a high-latitude area like Norway were somewhat expected, given the intrinsic strong points of the model. However, the robustness of the Linear Model's underlying physics was put succesfully under stress in the third paper, where the model performed well also at hourly time resolution at meteorological time scales. Last but not least, the fourth paper showed another way to exploit the Linear Model's features for climatological downscaling in warmer, mid-latitude regions.

1 Introduction

The problems posed by recent climate changes and the need for adaptation techniques in the near future have motivated many of the most recent efforts in climatology. Climatology is described by the US NOAA as "the description and scientific study of climate", or more precisely as "a quantitative description of climate showing the characteristic values of climate variables over a region" (http://www.cpc.ncep.noaa.gov/products/outreach/glossary.shtml). The main tools developed for future climate projections have been Global Climate Models (GCMs, from now on), which simulate the state of the climate over the Earth's surface (e.g., IPCC AR4, 2007). GCMs are used to understand climatological features and global changes. These include large scale distributions of precipitation, sea level pressure and surface air temperature, with a special attention to monthly means and seasonal variations. These variables and distributions have been chosen as indicators of climate change as they are simple to understand and measure, and because they are believed to give a generalized representation of climate. GCMs have been demonstrated to reproduce observed features of recent climate (IPCC AR4, Chapter 8). Their coarse resolution means that they are less realistic for smaller scale features, like those at less than the $\sim 150 - 200$ km scale; moreover, high resolution GCM runs are not feasible due to their high computational costs. In particular, GCMs are not able to resolve physics that lead to hydrological extreme events: heavy and extreme precipitation with

accompanying floods, flash floods and avalanches; droughts; salinization of coastal aquifers (e.g., Salathé Jr., 2005; Christensen and Christensen, 2007). However, impact researchers need local climatologies in order to provide policy makers with guidelines for implementing assessment policies.

Downscaling is used to obtain high-resolution, local projections of coarse-resolution GCM results. The main assumption behind the theory of downscaling is that large-scale weather exhibits a strong influence on local-scale weather, so that data from GCMs can be used to force (or drive) a model over a limited area (e.g.: Wigley et al., 1990; Giorgi and Mearns, 1999; Maraun et al., 2010; Rummukainen, 2010). The drawbacks of the technique include addititional uncertainty and high computational demands.

Precipitation is, with temperature, one of the most important variables for impact studies in meteorology and climatology. The role of precipitation in science (geophysics, hydrology, meteorology and climatology) and human activities is of fundamental relevance, from its impact on water budgets to farming, from river floods to droughts. Complex terrains (mountains, hills and plateaus) cover 46% of the Earth's land surface, contain 46% of the global population and produce 51% of the surface runoff (Meybeck et al., 2001), so mountain precipitation is especially important. Meyers and Steenburgh (2013) list orographic-precipitation-generated challenges to both science and human activities: i) snow and storms; ii) floods, landslides and debris flows; and iii) droughts. Moreover, Orographic Precipitation processes develop at spatial scales that require models to solve very high resolutions, possibly as

high as a few hundred meters. This is a problem not only for global climate models, which are provided generally at resolutions of 180-300 km, but often even for downscaling regional climate models, whose resolutions can be as high as 10-25 km - still too little to resolve the necessary physics.

During the last few decades, the application of high-resolution models and new observational field datasets, collected over topographic barriers around the world, have quantified various orographic processes for a broad spectrum of ambient environments and barrier dimensions (Colle et al., 2013, see Table 1). These experiments have helped the advance in understanding Orographic Precipitation so much that several reviews have been written in the last few years (Lin, 2005; Roe, 2005; Smith, 2006; Rotunno and Houze, 2007; Houze, 2012; Colle et al., 2013).

This study focuses mainly on one of the precipitation models created in these years, namely Smith and Barstad's Linear Model (LM, 2004). The LM provided a new, analytically simple and powerful tool to study Orographic Precipitation. The LM is a CPU-inexpensive, reduced model, so it can be used to perform high-resolution downscaling at virtually any desired spatial scale. It is a steady state model, so it can be used with input data of any time resolution. Its simple physics makes it possible to study a great range of changing parameters and variables. The LM has been used succesfully, alone or in conjunction with other models, in many forecasting and climatological studies in non-tropical areas, e.g. Oregon (Barstad and Smith, 2005; Smith et al., 2005); the Andes (Smith and Evans, 2007); Iceland (Crochet et al.,

Name	location	year(s)	main topics	sample ref.
Sierra Cooperative Project	Sierra Mountains	late 1970s - 80s	precipitation evolution / thermodynamics / microphysics over a wide barrier with landfalling storms	Reynolds and Dennis (1986)
TAMEX	Taiwan	1987	Mei-Yu front, mesoscale convective systems	Kuo and Chen (1990)
HARP	Hawaii	1990	diurnal variability of precipitation around isolated topography	Chen and Nash (1994)
COAST	Olympic Mountains	1993	precipitation and kinematic evolution over an isolated barrier	Bond and Coauthors (1997)
WISP	Front Range, Colorado	1990-1994	ice nucleation, supercooled water, precipitation evolution	Rasmussen et al. (1992)
SALPEX	Southern Alps, NZ	1996	precipitation over a narrow steep barrier	Wratt et al. (1996)
MAP	European Alps	1999	linking moist dynamcs in blocked / unblocked flow with precipitation distribution / processes	Rotunno and Houze (2007)
CALJET	California	1998	effects of topography in coastal precipitation enhancement, warm rain processes and atmospheric rivers	Neiman et al. (2002)
PACJET	Pacific US	2000-2001	(as CALJET, see above)	Ralph et al. (2005)
IMPROVE-2	Oregon, Cascade Mountains	2001	precipitation processes and microphysics	Stoelinga and Coauthors (2003)
IPEX	Wasatch Mountains	2001	precipitation processes, diabatic impacts, microphysics for a narrow barrier	Schultz and Coauthors (2002)
Southern Andes Project	Andes	2005	air mass transformation, isotope analysis	Smith and Evans (2007)
COPS	SW Germany	2007	orographically induced convective precipitation	Wulfmeyer et al. (2008)

Table 1: Measurement campaigns involving OP experiments. Adapted from Colle et al., 2013.

2007); Washington State (Anders et al., 2007); Norway (Schuler et al., 2008); Southern California (Hughes et al., 2009); and British Columbia (Jarosch et al., 2012).

Among the shortcomings of the LM pointed out by these studies are: i) the LM is a vertically integrated model, and thus misses stratification and layer details; ii) the model's use of constant time delays to describe conversion and fall-out times; iii) its linear airflow dynamics and simple microphysics are based on lifting, and a negative gradient in topography (i.e., downhill) tends to result in too little precipitation on the lee side. Schuller and Barstad (2011) tried to address the first issue by extending the theory through the introduction of vertical layers.

This study is going to give a thorough exploration of the LM's performance capabilities at the high resolutions required by current forecasting and climatological related studies of precipitation. In particular, this study will use the LM in areas of study that will put under stress the boundaries of its feasibility and try to answer these questions:

1) Are the simple physics of the LM enough to furnish credible high resolution data to use in climatological assessment studies? To answer this question, we must first and foremost find if (and where) the LM is able to reproduce past local climatological precipitation and whether its information adds to the previous knowledge obtained from GCMs.

2) How well does the LM compare with other, more complex models? Is the LM able to provide useful information beyond that provided by more

complex models? This question can be answered through the comparison of LM and: i) forecasting tools; ii) RCMs or other downscaling methods.

3) The LM has been used mostly in mid high latitudes and/or in areas where most precipitation is of orographic nature. Are there simple and effective ways to overcome this limitation and use the LM to contribute to a more general description of precipitation climatology in warmer climates? To do this, we must combine the LM with other methods in areas where an orographic description of precipitation is not enough to resolve precipitation climatology.

The thesis is structured as follows: sections 1.1 and 1.2 shortly introduce some general knowledge about saturation and cloud microphysics that is relevant to precipitation. Section 2 discusses Orographic Precipitation, with a special focus on the theoretical foundations of the Linear Model. Section 3 deals with elements of precipitation downscaling, and presents the downscaling methods used in this work, namely the Linear Model, the Multifractal Model, and Liston and Elder's downscaling scheme. Section 4 introduces and presents the results from the four papers that are included in this work. The four papers are included in the Appendix.

1.1 Saturation and Air Temperature

The ability of an air parcel to carry water vapour is of fundamental importance to precipitation. A parcel will become saturated (i.e., there is dynamical equilibrium between the liquid and gaseous states, i.e., its relative

humidity reaches 100%) if the partial pressure of the water vapour (e in the equation of state of water vapour, $eV_w = R_w T$) attains a threshold value e_s. This saturation vapour pressure is a sensitive function of temperature, given by the Clausius-Clapeyron relationship:

$$e_s(T) = 6.112 \exp(\frac{aT}{b+T}) \tag{1}$$

where e_s is measured in millibars, T in $^\circ C$, and the parameters are $a = 17.67$ and $b = 243.5^\circ C$. This expression is accurate to within 0.3% in the temperature range $-35^\circ C < T < 35^\circ C$ (e.g.: Bolton, 1980; Emanuel, 1994). A parcel of unsaturated air that encounters terrain and is forced to ascend will expand adiabatically as the environmental pressure drops and it will cool, and eventually the vapour it contains will reach saturation. At that point, the saturation specific humidity (the mass of saturated water vapour) becomes:

$$q_s(T, z) = 0.622 \frac{e_s(T)}{p(z)} \tag{2}$$

where $p(z)$ is the atmospheric pressure, so that q_s is a function of temperature and pressure only (e.g.: Wallace and Hobbs, 1977). If we make the approximation that atmospheric temperature varies linearly with height, then $T = T_0 + \gamma z$, where z is height, γ is called the temperature lapse rate, and T_0 denotes the temperature at height $z = 0$. If ρ is the air density, then the mass of water vapour per unit volume in a saturated air parcel can be

written (e.g., Matveev, 1967) as

$$\rho q_s(z) = \rho_0 q_{s_0} exp(-z/H_w) \tag{3}$$

where $H_w = -\frac{RT_0{}^2}{L\gamma}$ is called water vapour scale height, with $R = 461\ J\ Kg\ K^{-1}$ and $L = 2.5 \times 10^6\ J\ kg^{-1}$. It is a measure of the depth of the moist layer, and it generally varies between 1 and 5 km (see for instance: Smith and Barstad, 2004), with values being typically about 2 km for high-latitudes and about 4 km in the tropics (e.g., Roe, 2005). Vapour pressures within the atmosphere rarely exceed the saturation value by more than 1% (e.g., Houze, 1993), so for a saturated parcel of air ascending with vertical velocity w, the rate of condensation of water vapour is very close to the rate of change of the water vapour scale height:

$$-\frac{d(\rho q_s)}{dt} \simeq -\frac{\partial(\rho q_s)}{\partial z}\frac{dz}{dt} = -w\frac{\partial(\rho q_s)}{\partial z} \tag{4}$$

How and if condensation is precipitated depends on atmospheric response, cloud microphysics and on the ambient humidity of the air through which precipitation falls, which may cause partial or total re-evaporation.

1.2 Cloud Microphysics

Microphysical processes are of major importance in determining how condensation is distributed over the landscape as precipitation. One of the most

important microphysical characteristics of clouds is the number, density and size of cloud droplets. Clouds are formed of droplets of different size. Droplet concentration varies from tens of thousands of particles per cm^3 in clouds, to a few per liter in rain. The size of cloud elements determines the type of precipitation. Small cloud droplets, formed by vapour condensation in rising air, will be carried downwind by the ambient flow while undergoing a conversion into particles large enough to have a significant terminal fall speed under the effect of gravity (Uttal et al., 1988; Yau and Rogers, 1989; Yuter and Houze, 2003; Smith, 2006). A typical raindrop or snowflake has a mass a million times greater than a cloud droplet, so the conversion is a nontrivial step in the formation of precipiation. Current estimates of the conversion time τ_c range from 100 to 2000 s and depend on physical factors like temperature, aerosol content and turbulence (e.g., Sinclair, 1994; Robichaud and Austin, 1988; Smith, 2003; Smith et al., 2003; Smith and Barstad, 2004). Once precipitation hydrometeors have formed, they fall with terminal velocities V_t ranging from 1 ms^{-1} (light snow) to 2 ms^{-1} (typical snow) to 6 ms^{-1} (rain) to 8-10 ms^{-1} (heavy rain) to 50 ms^{-1} (exceptionally large hail stones) (Roe, 2005; Smith, 2006). The bulk-version fallout time τ_f depends on the terminal velocity and on the water vapour scale height of the hydrometeor clouds, $\tau_f = H_w/V_t$ (Barstad and Schuller, 2011). With cloud depths varying from 1 to 5 km, fallout times range from 100 to 2500 s (Sinclair, 1994; Smith, 2003; Smith et al., 2003; Smith and Barstad, 2004, e.g.:). Colder conditions and snow will favour the larger values (Smith, 2006), which is consisent with

the expected theoretical timescales from the various growth processes (e.g.: Houze, 1993).

2 Orographic Precipitation

The influence of orography over precipitation is that of modifying it from pre-existing weather disturbances; we can define Orographic Precipitation (OP) as the modification of rain, snow and other hydrometeors resulting from the interaction of moist flow with topography (Colle et al., 2013). In mid-latitude, cool-season climates, precipitation is generally controlled by the weather cycle, i.e., the quasi-periodic passing of frontal cyclones. With intervals from 4 to 7 days, these cyclones produce precipitation wherever they occur, but the patterns and amount of precipitation can be strongly modulated by terrain (Smith, 2006). In Europe, cyclones passing north of the Alps bring snowfall to the northern slopes in winter, while cyclones passing along the Mediterranean Sea bring heavy rains to the southern Alpine slopes. Average westerlies have little to do with these events (Buzzi et al., 1998). Orography influences condensation within the atmosphere by affecting the airflow. The airflow response can be stable or unstable if convection (buoyancy-driven overturning) is triggered. The most straightforward mechanism of Orographic Precipitation is stable upslope ascent: forced mechanical lifting of the air impinging on the windward flank leads to cooling of the air column, resulting in condensation and precipitation; descent in the lee leads

to warming and drying, and precipitation is suppressed. At the scale of large mid-latitude mountain ranges (e.g., 40 km wide, 1.5 km high), this is certainly a good first-order description of what is going on (e.g.: Smith et al., 2003; Roe, 2005). For this picture to be true, the airflow response must also be a solution to the equations of motion. Parcels of air tend to seek their level of neutral buoyancy: in a stable and stratified atmosphere, a forced vertical displacement, like that caused by air crossing orography from windward to leeward flanks, will create restoring forces that set up atmospheric gravity waves. These may propagate away from the source, or may decay exponentially away from the surface (e.g.: Smith, 1979; Durran, 1990). If the atmosphere is too stable or the flow is not strong enough, the flow may be blocked by orography, and then get diverted around the mountain or stagnate (Roe, 2005; Colle et al., 2013). Another possibility of atmospheric response to orography is the triggering of unstable convection (e.g.: Banta, 1990). If the orography lifts air above its level of free convection (the level at which the air becomes less dense than its surroundings), it will continue to rise. This unstable ascent enhances the condensation rate locally and can also produce great amounts of super-cooled cloud water droplets, causing the efficient fall-out of precipitation particles that would otherwise grow more slowly. Last but not least, we mention the possible effect of solar heating on sun-facing slopes, which is responsible for the afternoon thunderstorms in summer that occur in many mountainous regions (Roe, 2005). The common mechanism of all these phenomena is that orographic-induced ascent produces a condensa-

tion region - whether or not, in the end, that condensation produces ground precipitation. This mechanism has normally a self-destructing effect, as it kills the heating with precipitation and clouds.

2.1 Moist airflow dynamics

Precipitation tends to increase with the steepness of windward slopes owing to enhanced lifting and tends to decrease with elevation owing to the Clausius-Clapeyron effect (Roe, 2005). Using this basic physical concept, several theories of Orographic Precipitation have been proposed, starting with Hobbs et al. (1973), Fraser et al. (1973), Collier (1975), Colton (1976), Rhea (1978) and Smith (1979). The starting point for the analysis of Orographic Precipitation is the study of moist airflow dynamics and the realization that the nature of the terrain-induced ascent depends on the width a of the hill (e.g., Smith (1979)). The vertical extent of the atmosphere that feels the presence of the mountain is limited: for narrow hills ($a < 1km$), the vertical penetration of the forced ascent is no larger than the width of the hill. For wider hills, vertical penetration is influenced also by density stratification and latent heat release, a measure of which may be given by the Brunt-Vaisala frequency (the frequency at which an air parcel oscillates when it is subject to an infinitesimal perturbation in a stably stratified atmosphere):

$$N^2 = \frac{g}{T}[\gamma - \Gamma] \tag{5}$$

where g is gravity, T is the temperature, γ and Γ are the actual and adiabatic lapse rates, respectively. If $\gamma = -0.0065°C/m$, $\Gamma = -0.0098°C/m$, $T = 273$ K, then $N = 0.01s^{-1}$. The natural buoyant oscillation period of air is about 600 s. With air parcels wanting to return to their initial vertical level within ten minutes, simple ascent forced by sloping terrain is converted into a more complex gravity wave (e.g.: Smith, 1979; Wurtele et al., 1996). Gravity wave flow fields are characterized by upwind tilting patterns of airflow disturbances (see Durran (1990); Figure 7, in Roe (2005); Figure 2, in Smith (2006)). The strength and penetration depth of the forced vertical motion is limited by the phase tilt in these waves. The approximate penetration depth of the vertical motion, for simple 2D hydrostatic flow, is $z = U/N$ (see, for instance, figure 2 and pages 3-4 in Smith, 2006). Using, for example, wind speed $U = 10\ ms^{-1}$, and stability $N = 0.01s^{-1}$, this penetration height becomes approximately 1000 m. Air which passes over the hill above that level (in our example, for instance, around 2000 m of height) does not feel the terrain forced ascent.

If the terrain is very high, an approaching air mass may be decelerated and forced to split near the ground, and then flow around the mountain. This can affect and reduce the amount of forced ascent. Jiang (2003) showed that blocking-induced convergence dominates the windward lift, and that, especially for very high mountains, blocking may cause flow reversal over the windward slope with a secondary circulation.

Given flow speed U, stability N and mountain height h, we introduce a variable called the nondimensional mountain height (inverse Froude number)

M. Stability and nondimensional mountain height can be used to describe several cases of terrain-affected flow behaviour.

If $M = hN/U >> 1$, then some of the air will flow around the hill. Considering our previous example, for $U = 10\ m/s$ and $N = 0.01s^{-1}$, a mountain of 1 km of height or more will exceed this limit and flow splitting will result.

In saturated air, ascent triggers water vapour condensation and thus release of latent heat, which opposes the cooling associated with adiabatic expansion; thus, the buoyancy restoring force is decreased. Hence, for saturated air, Γ is replaced by the moist adiabatic lapse rate Γ_m, and N^2 is replaced by the moist stability frequency ${N_m}^2$ (e.g., Durran and Klemp, 1982; Barcilon and Fitzjarrald, 1985; Jiang, 2003). Durran and Klemp, (1982), for example, give the moist static stability as:

$$ {N_m}^2 = \frac{g}{T}\left(\frac{dT}{dz} + \Gamma_m\right)\left(1 + \frac{Lq_v}{RT}\right) - \frac{g}{1+q_w}\frac{dq_w}{dz} \tag{6} $$

where $q_w = q_v + q_c$ is the total water mixing ratio and q_v is the total water vapour mixing ratio, with q_c being the cloud water mixing ratio.

If we substitute $M = hN_m/U \lesssim 1$, then there are less or no flow blocking and more gravity waves over the windward ridges and the crest, which can influence precipitation distribution and enhancement up to 20% (Reinking et al., 2000; Colle, 2004; Garvert et al., 2007; Colle et al., 2008, 2013), even over the crest and in the immediate lee (Bruintjes et al., 1994). N_m varies

strongly with temperature: at about 280 K, typical values of N_m are about 1/2 or 1/3 of those N takes at the same temperature, while there is almost no difference between them at about 240 K. This means that, due to the release of latent heat with condensation, moist air can theoretically ascend over mountains up to twice the height reached by dry air (Jiang, 2003; Smith, 2006). This also means that the ascent will catch a much bigger fraction of the moisture flux across the terrain. When descent starts, any condensed water that has not converted and precipitated is subject to evaporation.

Although the simple substitution of N with N_m has provided good results (e.g.: Jiang, 2003), predictability issues still remain, as other parameters might influence flow perturbations (Reeves and Rotunno, 2008; Colle et al., 2013); last but not least, other problems not solved by the introduction of a moist stability are posed by horizontal gradients in the moisture (Rotunno and Ferretti, 2001) or regions of latent heating (Galewsky and Sobel, 2005).

As an example, let us consider a ridge with a half-width of $a = 10$ km. With a wind speed of $U = 10\ m\ s^{-1}$, the time it takes a parcel to travel from the foothill to the crest is $t = a/U = 1000$ s. If the conversion time for a parcel from vapour to liquid state (τ_c) and the fallout time for a particle (τ_f) are $\tau_c = \tau_f = 200$ s, conversion and fallout will be completed before descent begins. If $\tau_c = \tau_f$, only a small fraction of the condensed water will precipitate; the rest will evaporate on the lee side.

If $N_m \sim 0$ and saturation is reached, then simulations show that there is zero blocking and long vertical wavelengths are achieved (Miglietta and

Rotunno, 2005, 2007). Moist neutral stratifications up to about 3 km above sea level were observed in field projects (Rotunno and Ferretti, 2003; Ralph et al., 2005).

2.2 Linear Model of Orographic Precipitation

The primary ingredients for Orographic Precipitation include: i) ascent over the barrier (upslope, gravity waves, and large-scale ascents); ii) water vapour flux; iii) microphysical growth and conversion (Colle et al., 2013). In this section we will follow the development by Smith and Barstad of a linear steady-state theory for Orographic Precipitation. Their model, called Linear Model (LM), includes linear airflow dynamics, cloud physics and their relationship with barrier dimensions (Jiang and Smith, 2003; Smith and Barstad, 2004; Smith et al., 2005; Smith, 2006).

2.2.1 Upslope model

The simplest possible model for the condensed water source term (Colton, 1976; Rhea, 1978; Smith, 1979) is:

$$S(x,y) = \rho q_v \vec{U} \bullet \nabla h(x,y) \tag{7}$$

under the assumptions that i) the vertical air motion is independent of height, ii) the air is saturated with vapour, iii) the temperature sounding follows a saturated moist adiabat, iv) the fall-out is instantaneous. The

factors ρ and q_v are the air density and specific humidity at the Earth's surface.

As a propotype physical model of cloud physics, Smith (2003) considers a pair of steady-state equations which describe the horizontal advection $\vec{U}$ of vertically-integrated condensation water:

$$\vec{U} \bullet \nabla q_c = S(x, y) - q_c/\tau_c \tag{8a}$$

$$\vec{U} \bullet \nabla q_f = q_c/\tau_c - q_f/\tau_f \tag{8b}$$

where S is the source term, i.e. the rate at which supersaturated water vapour (=cloud water) is generated by ascent (=moist adiabatic uplift). Cloud water and hydrometeor column densities q_c and q_f are in units of $kg\ m^{-2}$. In these equations, q_c/τ_c is the mass of cloud water converted into hydrometeors, while $P(x, y) = q_f/\tau_c$ is the fallout of hydrometeors on the ground, or precipitation. If we assume that the conversion and fallout are instantaneous ($\tau_c = \tau_f = 0$), then $P(x, y) = S(x, y)$. This model is referred to as the raw upslope model. As forced ascent makes S positive, the amount of cloud water increases downwind. The conversion term in Equation (8a) then acts to decrease the amount of cloud water and generate rain water. Nonetheless, (7) still has ambiguities (Colle et al., 2013) as: i) it is not defined what sort of wind one should use for $\vec{U}$(e.g., 10 m wind, 925 hPa wind); ii) it is not defined which slope one should use for ∇h.

2.2.2 Smith and Barstad's Linear Model

Smith and Barstad (2004) presented a highly adaptable quasi-analytical OP model incorporating a linear atmospheric response that is capable of efficient calculation over complex terrain. Cloud microphysics are represented in their model by characteristic time delays for hydrometeor growth and fallout.

The starting point of their work comes from Smith (2003), who solved the precipitation and source equations of the previous section. He did so by Fourier transforming each variable field, obtaining an expression for the FT-precipitation distribution

$$\hat{P}(k,l) = \frac{\hat{S}(k,l)}{[1 + i\sigma\tau_c][1 + i\sigma\tau_f]} \tag{9}$$

where k and l are the components of the horizontal wavenumber vector. We can then inverse-Fourier-transform Equation (9) to obtain the precipitation distribution in the normal space (x, y).

Note that (9) has two important mathematical properties:

1) If the input source $S(x, y)$ is everywhere positive, then $P(x, y)$ will be positive also. This means that, as ascent always makes S positive, it results in an increase of cloud water (and possibly precipitation).

2) The area integrals of $S(x, y)$ and $P(x, y)$ are identical - the advection and time delays serve only to re-distribute precipitation (Smith, 2003).

To prevent the source from becoming a sink in Equation (7) when downsloping occurs in an unsheared saturated moist-neutral atmosphere, Smith intro-

duces $S(x,y) = Max(S,0)$.

The source term corresponds to the horizontal water vapour flux $\vec{U}$, i.e., the rate at which water vapour is carried horizontally past a point in a layer above the earth's surface.

If the moist lapse rate Γ_m is assumed to be constant, Smith and Barstad (2004) propose as source the term

$$S(x,y) = C_w \vec{U} \bullet \nabla h(x,y) \tag{10}$$

where C_w is the uplift sensitivity factor (the coefficient relating condensation rate to vertical motion) $C_w = \rho_{Sref} \frac{\Gamma_m}{\gamma}$, with $\rho_{Sref} = e_S(T_{ref})/RT_{ref}$; e_S is the saturation vapour pressure at the temperature of the ground T_{ref}, and $R = 461 Jkg K^{-1}$ is the gas constant for vapour, while γ is the environmental lapse rate, $\gamma = \frac{dT}{dz}$.

If we i) assume saturated conditions, ii) include wave dynamics, iii) neglect Coriolis, we have $\sigma = Uk + Vl$ as the intrinsic frequency, $m(k,l) = [(\frac{{N_m}^2 - \sigma^2}{\sigma^2})(k^2 + l^2)]^{1/2}$ as the vertical wavenumber and $H_w = -R\frac{{T_{ref}}^2}{L\gamma}$ as the water vapour scale height (with $L = 2.5 \times 10^6 Jkg^{-1}$ being the latent heat; see also Section 1.1). Then in Fourier space (10) becomes

$$\hat{S}(k,l) = \frac{C_w i\sigma \hat{h}(k,l)}{(1 - imH_w)} \tag{11}$$

If we consider the steady state advection (8a and 8b), and the source term in Fourier space, by applying simple algebra we can obtain an expression for

the Fourier transform of the precipitation distribution $\hat{P}$ that relates the terrain height $\hat{h}$ to the precipitation field $\hat{P}$:

$$\hat{P}(k,l) = \frac{iC_w\sigma\hat{h}(k,l)}{(1-imH_w)(1+i\sigma\tau_c)(1+i\sigma\tau_f)} \tag{12}$$

which is dependent on the source $S(x,y)$ and considers time delays (the conversion and fall-out terms τ_c and τ_f). The denominator factor $(1-imH_w)$ contains the effect of vertical velocity variations through the moist layer, while the other two factors contain the contribution of cloud delays (through τ_c and τ_f) and advection (through σ) (e.g.: Smith and Barstad, 2004)). The precipitation intensity distribution is then obtained through an inverse Fourier transform.

Since the water vapour density is $\rho_S(T) = e_S(T)/(RT)$, with $e_S(T)$ given by the Clausius-Clapeyron equation $e_S(T) = e_{S_{ref}} e^{L\Delta T/RT_{ref}{}^2}$ and L $\Delta T/RT_{ref}{}^2 = -z/H_w$, we can approximate the vertical distribution of water vapour for $T \sim T_{ref}$:

$$\rho_s(z) = \rho(T_{ref})e^{-z/H_w} \tag{13}$$

Smith and Barstad's OP Linear Model benefits from the following properties:

- it is analytically tractable, so its properties are easily understood;
- it is applicable to complex terrain and arbitrary wind directions, and

thus can be tested against real data;

- it reduces to the classical upslope model, so it can be compared with earlier work;
- it includes airflow dynamics, condensed water conversion, advection and fallout, and downslope evaporation;
- the ambiguity around $\nabla h(x, y)$ in (7) is gone as the wave dynamics damp disturbances that are too short;

  but it also has the following limitations:

- it is limited to modest mountain heights where $M \ll 1$ and the drying ratio $DR = \frac{P}{S}$ (i.e., total precipitation divided by vapor influx) has to be $DR \ll 1$;
- it cannot account for flow blocking or unstable conditions;
- it is vertically integrated, so it cannot account for vertical variations of atmospheric variables like wind, moist static stability, density and humidity;
- it uses constant time-delays, thus being unable to describe complex variations in microphysics aloft;
- it is intrinsically deficient in its description of lee-side precipitation.

It is also important to remember that the use of steady state equations means that there really is not a temporal resolution in the model; there is

rather a time frame over which the model calculates precipitation intensities. The model can thus operate at any given time frame, depending on the format of the input data. The precipitation intensity over the time frame can also be calibrated: it can be assumed that it will rain for the whole time frame or just for a part of it. This calibration can be incorporated in the model code or be implemented in the post-processing phase.

The transparent nature of the linear model makes it a promising, fruitful choice as a diagnostic tool for climatological studies about Orographic Precipitation. Remembering that $H_w = -R\frac{{T_{ref}}^2}{L\gamma}$ is the water vapour scale height, assuming that $\gamma < 0$, the column-integrated water vapour is $\rho_{Sref}H_w$ and the horizontal flux of water vapour advected by a constant wind is:

$$\vec{F} = \rho_{Sref}H_w\vec{U} \tag{14}$$

By using (14) we can re-write the source term for moist air in (10) as:

$$S = \frac{\Gamma_m}{\gamma}\frac{\vec{F}}{H_w} \bullet \nabla h(x,y) = \rho_{Sref}\frac{\Gamma_m}{\gamma}\vec{U} \bullet \nabla h(x,y) \tag{15}$$

Using the relationship between the lapse rates and moist static stability (Fraser et al., 1973), we get $\Gamma_m = \gamma - \frac{N^2T}{g}$ and $\gamma = -\frac{RT^2}{LH_w}$, and by substituting these in Equation (15) we get:

$$S(x,y) = \rho_{Sref}[\frac{N^2H_wL}{gRT} + 1]\vec{U} \bullet \nabla h(x,y) \tag{16}$$

The precipitation intensity will thus be given by the Fourier inverse trans-

form of

$$\hat{P}(k,l) = \frac{i\rho_{Sref}\sigma[\frac{N^2 H_w L}{gRT} + 1]\hat{h}(k,l)}{(1 - imH_w)(1 + i\sigma\tau_c)(1 + i\sigma\tau_f)} \tag{17}$$

Notwithstanding orography, the changes in the source term (16) and in precipitation intensity (17) will be fully determined by the change in temperature, moist stability, and wind speed and direction. This allows, for example, to determine a direct relationship between the change in major climatological parameters (like average temperature and storminess) and changes in total and extreme precipitation (e.g.: Caroletti and Barstad, 2010)).

3 Precipitation Downscaling

There are two main categories of downscaling: dynamical downscaling, which is based on nesting a Regional Climate Model (RCM) into a GCM to represent the atmospheric physics at a higher resolution (e.g. Déqué and Piedelievre, 1995; Rummukainen, 1997; Giorgi and Mearns, 1999; Xu, 1999; Rummukainen, 2010); and statistical downscaling, which is based on finding statistical links between large-scale weather and observed local-scale weather (see e.g. Wilby et al., 1998). It is important to note that, in practice, most downscaling approaches tend to be hybrid in nature, as a combination of several methods can better address the shortcomings of a single technique (Haylock et al., 2006; Schmidli et al., 2007).

Dynamical downscaling methods contain the same representations of at-

mospheric processes as global models. Among the most common approaches are: i) running a RCM with coarse GCM data or reanalysis data as boundary conditions ('one-way nesting'); ii) performing global-scale experiments with high-resolution Atmosphere GCMs (AGCMs) - which lack the ocean-atmosphere feedbacks present in full GCMs - using coarse GCM data as initial and boundary conditions; iii) using a variable-resolution global model (with highest resolution over the area of interest).

RCMs have a horizontal resolution in the order of tens of kilometers (typically they have 25-50 km resolution grids). A RCM must cover a large enough area to allow phenomena related to topography and small-scale atmosphere processes to develop. A properly run RCM can i) give rise to local and regional circulation and precipitation features, ii) modify temperature and winds, and iii) improve the simulation of synoptic and mesoscale systems including fronts and precipitation extremes.

When GCM data are used as boundary conditions, maximum values tend to increase and be more realistic, and there is an improvement in the representation of daily variations and distribution (e.g. precipitation). However, significant biases of the driving GCMs are fully inherited, and for some variables, like precipitation, extreme values are not well-represented. A worrying theoretical problem about GCM-RCM downscaling lies in the parametrization schemes used in GCMs, that might not be appropriate for use in RCMs - for example, their specific nature and the extent to which they are needed depend on model resolution (e.g., Lenderink and Van Mei-

jgaard (2008): precipitation in the summer and on sub-daily scales, when highest precipitation intensity is more of a convective nature; Hohenegger et al. (2008): parametrization schemes developed for coarse and/or tropical regions).

Another possibility for driving RCMs is to use reanalysis data as boundary conditions. This allows to exclude the systematic biases found in GCMs, and to reproduce day-to-day sequences of weather events (ERA40). The need for observations limits model evaluation, and the reanalysis approach will naturally be confined to past periods, and cannot be used for future projections.

RCMs consist of gridded data, while station observations are point data. This is a complication in particular for the evaluation of extremes, as gridded data are more homogenous in space than station data, so that extremes are typically attenuated.

Statistical downscaling, a computationally less demanding approach, is based on regional-scale atmospheric predictors (e.g.: area averages of precipitation or temperature) and circulation characteristics (e.g.: mean sea level pressure or vorticity) that are related to station-scale meteorological series through statistical relations. Statistical downscaling can be used for downscaling GCMs or even RCMs. In comparison with RCMs, statistical downscaling has the advantage of demanding less CPU time and resources. However, since it is not based on physics, it is much more dependent on the results of the driving model than physical downscaling. Common assump-

tions needed for all types of statistical downscaling methods are: i) local-scale parameters are a function of synoptic (i.e., large-scale, $\sim$ 1000 km) forcing; ii) the GCM used to derive relationships must be valid at the scale used; iii) the relationship derived must remain valid under greenhouse forcing.

The main epistemological problem with the downscaling of climate models is finding a way to

1) control and limit the increase in uncertainty when resolution is increased;

2) make techniques as general as possible, to make them applicable to a wide range of conditions and areas and favour intercomparison;

3) be most effective (making it easy to reproduce and perform many tests, having little computational demand and great analytical power), in order to be able to simulate across scenarios and across GCMs. All scenarios must be downscaled, otherwise not all the uncertainties of the climate system will be represented and taken into account.

Full models are too expensive to fulfill all these requirements, so very often they are employed to study special cases or just a part of the climate scenarios, thus climate assessments might suffer from this. A reduced model, on the other hand, may be able to analyse a full range of possibilities and span the whole range of uncertainties. Smith and Barstad's Linear Model is a reduced model, and in this thesis we have worked to prove its capabilities in climate scenarios and model validation/intercomparison both at climatological and meteorological time scales.

In the following sections, we will shortly describe three downscaling methods that we have employed in the present work: Smith and Barstad's Linear Model, Deidda's Multi-Fractal Model, and the use of a two-step interpolation scheme for precipitation by Liston and Elder (2006).

3.1 Downscaling OP with the Linear Model

Essentially, the Linear Model (described in full in Section 2.2) makes use of a simple set of equations to describe the advection of condensed water by a mean wind (Smith and Barstad, 2004). The Linear Model can thus be used to downscale Orographic Precipitation by calculating it over a grid fed with GCM, RCM or other simulation data, obtaining precipitation intensities. In real cases, climatological studies have been used to evaluate how to feed an appropriate $\vec{U}$ to the model; e.g., the choice of GCM grid points to provide input data for western Norway was based on the notion that water vapour transport is mainly from a sector extending from south to west.

The LM has been used successfully in idealised (e.g., Barstad et al., 2007) and realistic (e.g., Crochet et al., 2007) studies predicting orographic-induced precipitation. In upwind scenarios, LM compares favorably with more elaborate numerical models despite heavily simplified physics (e.g., Barstad et al., 2007), and simulated precipitation is in good agreement with observations (e.g., Crochet et al., 2007). The efficacy in calculating extreme events is comparable with ERA-40 reanalysis when the moisture is moved upwind (e.g., Caroletti and Barstad, 2010).

3.2 Deidda's Multi-Fractal Model

Deidda (2000) introduced a statistical MultiFractal (MF) model which can use as input any precipitation intensity from model simulations. It conserves total precipitation over the downscaling area but re-distributes it at a higher space and time resolution. The model thus assumes the initial precipitation intensities as correct over an area, but it is able to provide a precipitation breakdown both spatially and temporally over the region.

Multifractal theory has been described and used as a suitable framework for precipitation downscaling in several papers (Lovejoy and Mandelbrot, 1985; Schertzer and Lovejoy, 1987; Gupta and Waymire, 1993; Over and Gupta, 1994; Perica and Foufoula-Georgiou, 1996). Spatiotemporal precipitation can be well approximated by a self-similar multifractal process. Self-similarity corresponds to the Taylor hypothesis (Taylor, 1938); when applied to precipitation, it means that rainfall is forced by a large-scale advection velocity U that is constant at any space scale λ, so that $\tau_{MF} = \lambda/U$ holds for precipitation over a wide range of spatial and temporal scales.

Thus, we can define instantaneous precipitation P over an area $\lambda_x * \lambda_y$ in a time τ_{MF} as

$$P_{ijk}(\lambda_x, \lambda_y, \tau_{MF}) = \int_{x_i}^{x_i+\lambda_x} d\xi \int_{y_j}^{y_j+\lambda_y} d\theta \int_{t_k}^{t_k+\tau_{MF}} d\sigma i(\xi, \theta, \sigma) \qquad (18)$$

where $i \equiv i(x, y, t)$ is an instantaneous and continuous function describing

rainfall intensity.

To apply the theoretical multifractal model to a real case, a log-Poisson stochastic generator has been used (Deidda, 1999, 2000; Badas et al., 2006). The parameters needed by the generator are obtained by performing a calibration, through the use of real precipitation events. For example, in the fourth paper presented in this study, the calibration used was performed through a dense network of 1 minute resolution rain gauge measurements over southern Sardinia from 1986 to 1996, on a space grid of 13 km x 13 km.

The main disadvantage of the model is that it relies heavily on the initial data quality. The fact that it is a calibrated statistical model is both an advantage and a disadvantage: much time and a high-quality observation network are needed for the calibration of any area of interest before the model can be used; however, calibration is also the reason why the MF method has proven quite reliable in reproducing local climatologies in test case studies (Badas et al., 2006; Deidda et al., 2006; Mascaro et al., 2010, 2011).

3.3 Liston and Elder's precipitation downscaling scheme

This statistical method is used to downscale observations or simulation data. Downscaling is divided into two steps: first it follows the Barnes objective analysis interpolation scheme to get interpolated grid-point elevation and precipitation values, and then it calculates the precipitation following Liston and Elder's scheme (2006).

The Barnes objective analysis scheme (Barnes, 1964, 1973; Koch et al.,

1983) applies a Gaussian distance-dependent weighting function, in which the weight of the contribution of a given station to the overall value of the grid point decreases with increasing distance from the point.

The interpolation weight w is given by

$$w = exp[-\frac{r_w}{f(dn)}] \tag{19}$$

where r_w is the distance between the original grid point and the downscaling grid, while $f(dn)$ is the filter parameter whose value defines how smooth the interpolated field will be. This filter parameter is determined by data spacing and distribution (see Koch et al., 1983)).

Liston and Elder's scheme is:

$$P = P_0[\frac{1 + \chi(z - z_0)}{1 - \chi(z - z_0)}] \tag{20}$$

where P_0 is the interpolated grid-point precipitation, z_0 is the interpolated grid-point elevation surface, and χ, expressed in km^{-1}, is a monthly-varying factor (Thornton et al., 1997).

The main advantage of the method is that, by using a Barnes scheme, it is able to downscale non-regular grids, or simulations with missing data, producing regular sets of downscaled data. However, the downscaling is driven only by simple topographic relationships. Another disadvantage is that, like in the Multifractal method, downscaling results are heavily dependent on the quality of input data, but, since this is not a calibrated method, they are not

improved by knowledge of local climatology.

4 Precipitation timescales

Jiang and Smith (2003) note that mountain areas are good for studying cloud microphysics and precipitation because the dynamical forcing by mountains is relatively well defined. The precipitation efficiency seems to depend on the moisture content of the incoming flow (increasing with moisture content in low-level flow), mountain size (increasing with mountain size) and mountain locations (becoming larger for coastal mountains).

Bergeron (1960) described the importance of advection timescales, since advection over a small hill might not take enough time to allow hydrometeor formation.

Jiang and Smith (2003) have tested timescales describing several processes: advection over orography, fallout, and snow generation. Typical conversion times from cloud water to rain are between 200 s and 2000 s (Houze, 1993; Smith, 2003); longer residence times within clouds result in precipitation delay. Conversion times in the $900 - 2000$ s time region would imply that stable flow over a narrow mountain or hill ($a < 10 - 20$ km) does not have enough time to produce precipitation enhancement (Houze, 1993; Colle et al., 2013). However, in the presence of a widespread frontal cloud, precipitation can become enhanced via a seeder-feeder mechanism even over small hills ($50 - 200$ m), a process in which precipitation particles falling from

aloft (seeder cloud) grow via accretion as they collect small cloud droplets within the low level cap cloud (feeder cloud) over a hill (Bergeron, 1949, 1960, 1965; Browning et al., 1975; Storebo, 1976; Houze, 1993; Colle et al., 2013). If precipitation fallout is rapid with riming ($2-4\ ms^{-1}$), then the microphysical time scale is relatively short and even relatively narrow barriers can have large precipitation rates and drying ratios. Let us take for example snow falling at $w \sim 1\ ms^{-1}$ from 2 km above the mountain slope: it will drift downwind 20 km, and thus it will quickly fall into the lee of a 10 km wide barrier, although a fraction of this lee precipitation will evaporate or sublimate (Colle et al., 2013).

The time delay $\tau = 1000\ s$ summarises combined effects of cloud physics processes (Barstad and Smith, 2005), and has been used for the Linear Model in many regional studies (e.g., Smith, 2006; Crochet et al., 2007)). Longer time delays imply more precipitation advected past steep topographic regions, and thus there will be i) increased precipitation on the lee side of the topography and ii) lower overall precipitation intensity. Shorter time delays result in an upwind shift of the more intense rain (Smith and Barstad, 2004; Barstad et al., 2007).

Inappropriate timescales can dramatically alter the accuracy of an experiment. Most earlier studies have used constant conversion and fallout timescales, trying to find a way to limit the arbitrariness of the choice, for example by calibrating the mean timescale with precipitation data. By using the properties of the Linear Model, however, it is possible to try another

route by calculating the timescales analytically.

We can reconstruct the conversion times of the precipitated droplets from the Orographic Precipitation, given by Equation (12):

$$(1 - imH_w)(1 + i\sigma\tau_c)(1 + i\sigma\tau_f)\hat{P}(k,l) = C_w i\sigma\hat{h}(k,l) \tag{21}$$

from which we get, by separating the real and imaginary parts:

$$1 - \sigma^2\tau_c\tau_f + m\sigma H_w\tau_f + m\sigma H_w\tau_c = 0 \tag{22}$$

$$\hat{P}[\sigma\tau_f + \sigma\tau_c - mH_w + m\sigma^2 H_w\tau_c\tau_f] = C_w\sigma\hat{h} \tag{23}$$

If we define the fallout time (Barstad and Schuller, 2011) as

$$\tau_f = \frac{H_w}{V_T} \tag{24}$$

where H_w is the water vapor scale height and V_T is the fallout speed of hydrometeors, fallout time becomes a known variable and, eliminating the integrals in the Fourier-transform since $\hat{P}$ and $\hat{h}$ are taken at the same point (k,l), we can obtain two possible formulations for the conversion time:

$$\tau_c = \frac{1 + \sigma m H_w\tau_f}{\sigma^2\tau_f - mH_w\sigma} \tag{25}$$

and

$$\tau_c = \frac{\frac{C_w \sigma h}{P} + mH_w - \sigma\tau_f}{\sigma + m\sigma^2 H_w \tau_f} \tag{26}$$

The denominator in Equation (25) also tells us that, in order to have conversion, we need the condition

$$\sigma\tau_f > mH_w \tag{27}$$

to be satisfied.

By using Equation (26), the LM can then be set to calibrate τ_c and τ_f, for instance using Orographic Precipitation data from a chosen station. However, we want to calculate τ_c with Equation (25) in order to have values that are independent of local orography and precipitation.

Typical ranges for m, H_w and σ can be found in the literature (e.g., Smith and Barstad, 2004; see Table 2). Fallspeed for rain ranges from 4 to 7 ms^{-1}. Values for liquid precipitation fallspeed can be found directly or indirectly in several papers (e.g., Berry and Pranger, 1974; Yuter et al., 2006). Using for instance $V_T = 6\ ms^{-1}$ for rain converted at 1200 m of height, we get $\tau_f = 200\ s$.

Table 3 shows results for τ_c obtained with Equation (25), varying σ and m and using $H_w = 1200$ and $\tau_f = 200\ s$. These results are in good agreement with the usual values in the literature and with other theoretical calculations in the same conditions. For example, Barstad and Schuller (2011) have τ_c between 500 and 750 s with $\tau_f = 164\ s$ for rain at heights of 1200 to 1500 m.

Name	Symbol	Typical range
Water vapour scale height	H_W	1 to 5 km
Intrinsic frequency	σ	0.01 to 0.0001 s^{-1}
Vertical wavenumber	m	0.01 to 0.0001 m^{-1}

Table 2: Typical values of vertical wavenumber, water vapour scale height and intrinsic frequency. Adapted from Smith and Barstad, 2004.

τ_c	$m = 0.0001$	$m = 0.0002$	$m = 0.0003$	$m = 0.0004$
$\sigma = 0.003$	744 s	1059 s	1689 s	3578 s
$\sigma = 0.004$	403 s	532 s	732 s	1081 s
$\sigma = 0.005$	254 s	326 s	425 s	569 s
$\sigma = 0.006$	176 s	224 s	284 s	365 s
$\sigma = 0.007$	130 s	164 s	206 s	260 s

Table 3: Examples of conversion time calculated with Equation 25. $H_w = 1.2$ km, rainfall velocity $V_T = 6ms^{-1}$, $\tau_f = 200$ s.

As an alternative method, we can consider $\tau_f = \tau_c = \tau$; thus, from Equation (22) and (23) we get two second order linear equations, whose only acceptable solutions are the positive ones because τ has to be a positive quantity. The solutions are

$$\tau = \frac{mH_w}{\sigma}(1 + \sqrt{1 + \frac{1}{m^2 H_w^2}}) \tag{28}$$

and

$$\tau = \frac{-1 + \sqrt{1 + mH_w(C_w \sigma \frac{h}{P} + mH_w)}}{m\sigma H_w} \tag{29}$$

Once again, we want a general solution that is valid for all points over the orography and does not depend on precipitation, so we consider only

τ	$m = 0.0001$	$m = 0.0002$	$m = 0.0003$	$m = 0.0004$
$\sigma = 0.003$	376 s	423 s	474 s	530 s
$\sigma = 0.004$	281 s	317 s	356 s	397 s
$\sigma = 0.005$	225 s	253 s	285 s	317 s
$\sigma = 0.006$	188 s	211 s	237 s	265 s
$\sigma = 0.007$	161 s	181 s	203 s	227 s

Table 4: Examples of timescales τ calculated with Equation (28). $H_w = 1.2$ km, $\tau_f = \tau_c$.

solution (28). Also in this case we calculate the theoretical values for this model, using the same ranges as above (see Table 2) and $H_w = 1.2$ km. The results, shown in Table 4, are consistent with the $150 - 200$ s values for the smallest timescales used in literature (e.g., Houze, 1993) and with the results obtained with the first method described above in this section.

Thus, to sum up the two possible means to calculate timescales using the physics of the Linear Method: the first method is to consider τ_f a parameter, obtained using V_T coming from the literature or from measurements, and then calculating τ_c; the second method is to set $\tau_c = \tau_f = \tau$ and then calculate τ.

5 Paper Presentation

This thesis used Smith and Barstad's LM in high-resolution studies, both meteorological and climatological, focusing on its possibilities in the topics of model validation and quick intercomparison of prediction methodologies at different timescales.

First and Second Papers

The first and second papers introduced the topic of climatological model validation, showing that RCMs are generally not good enough to properly resolve precipitation at the level of detail needed for climate assessment, especially on complex terrains such as the Alps. Downscaling is needed in order to increase the spatial and temporal resolution of RCMs, and to properly account for the physical processes that resolve precipitation and temperature in complex orography. The Linear Model was introduced as a valid downscaling option for climate studies in high-latitudes areas.

The first paper ("Regional climate models' performance in representing precipitation and temperature over selected Mediterranean areas") started as a model evaluation of fourteen EU-FP6 ENSEMBLES Global Climate Models/Regional Climate Models combinations, run for the A1B emission scenario at about 24 km grid resolution. The objective was to rank the performance of the models at six selected Mediterranean hydrological basins for the EU FP-7 CLIMB project. Observations used for the evaluation were taken from the E-OBS data set. Model evaluation was performed by introducing a metric constructed through precipitation and temperature errors at six Mediterranean hydrological basins. The validation period was 1951-2010.

The study showed how even the ENSEMBLES state-of-the-art RCMs had too coarse a resolution to reproduce in detail observed features of the catchments, both at precipitation and temperature level. This was especially true for the more orographically complex basins (i.e., the Noce catchment, in the

Italian Alps). The paper also described shortly the features of downscaling techniques used to bridge the gap between RCMs and observations in latter stages of the CLIMB project itself. These included the Multifractal method and Liston and Elder's downscaling scheme.

In the second paper, "An assessment of future extreme precipitation in western Norway using a linear model", we moved from the Mediterranean to Norway, in order to test the possibilities of the Linear Model as a method for climatological downscaling in an area where precipitation is mostly orographic in nature. First of all, we proved that in western Norway precipitation can be approximated with Orographic Precipitation for climatological studies, by comparing ERA40 reanalysis and model simulations in the 1971-2000 control period.

Thus, we used the LM for downscaling GCMs at resolutions of about 250 km down to a resolution of 1 km. Twelve IPCC AR4 Global Climate Models were downscaled over Southern Norway to produce a future assessment of precipitation extremes in the 2046-2065 and 2081-2100 time frames. Extreme precipitation was defined as events that exceed the 99.5% intensity threshold for the considered time frames. The future projections showed that extreme precipitation events were up to 20% more intense in future time periods when compared to 1971-2000 values. This result was consistent with other studies on high-latitude effects of global warming; however, the high resolution used allowed us to present individual assessments of rain stations, whose robustness was based on the good results and effectiveness in reproducing local

differences that were demonstrated for precipitation patterns throughout the control period.

The Linear Model was also used to disaggregate simulated changes in precipitation into the changes in the amount of moisture delivery to the area, and finally into changes due to temperature, wind speed or moist static stability. The study pointed towards the role of warming and increased static stability as the main drivers in the change in extreme precipitation intensity.

Third Paper

The third paper in the thesis ("Orographic precipitation across an island in southern Norway: model evaluation of time-step precipitation") dealt with high-space-and-time-resolution modelling of precipitation in complex topography on the meteorological time scale. The study compared WRF and LM simulations over a 12-week-long observation campaign on Stord, an island outside the Norwegian south-western coast. The WRF simulations suggested a significant convective component of precipitation, and performed well in reproducing the number of rain occurences at 1h, 3h and 24h accumulation intervals. However, the modelled precipitation for the campaign was only 60%-90% of the total observed precipitation. WRF simulations proved significantly better at reproducing the time-step precipitation intensities when used at a 1 km resolution than at a 3 km resolution.

The much simpler LM compared well with WRF in simulating 3-hour Orographic Precipitation at a 1 km resolution grid. We concluded that, in

general, the 1 km grid is enough to capture the most intensive precipitation both for WRF and the reduced LM.

Fourth Paper

The fourth paper, "Orographic corrections of climatological precipitation downscaling combining a physical based Linear model and a Multifractal model", aimed at testing orographic correction methods to produce high-resolution climate downscaling. This study also built on results from the first and second paper.

The area of study was the Riu Mannu hydrological basin in Sardinia (among those examined in the first paper that constitutes this thesis). Compared to the Norwegian case studied in the second paper of this thesis, Sardinian precipitation cannot be considered mainly orographic in nature, so a spatially homogeneous statistical method, the Multifractal model, was used for the initial background downscaling. Then two correction methods were used: the first one is a multiplicative modulated correction implemented directly in the Multifractal model; the second one is a novel method which added to the background field an orographic correction based on the Linear Model. The input data were the outputs of the four ENSEMBLES models selected in the first paper.

We studied the performance of the two orographic corrections and of the uncorrected statistical method when compared to E-OBS areal data and to station observations for the 1981-1990 time frame. We studied daily distribu-

tion, monthly means and yearly totals, and saw that both corrected methods performed better than the uncorrected Multifractal model at reproducing total intensity and monthly distributions at areal level and station level.

The good results of the LM proved our initial assumption that, for Sardinia, total precipitation can be approximately considered equal to the sum of Orographic Precipitation and a background component that includes large-scale and other effects. We thus concluded that: i) it is strongly advised to implement an orographic correction when using a spatially homogeneous statistical downscaling model; ii) locally triggered Orographic Precipitation in the Riu Mannu basin can be considered independent of other disturbances in first approximation.

The 1 km resolution proved to be enough to capture fairly well local intensities and distributions. Tests with a 250 m resolution did not produce more accurate results.

For this thesis it was especially important to see that the results of the novel method compared favourably with results from the painstakingly calibrated, modulated Multifractal downscaling in the same catchment. This suggested the possibility of a careful extension in the use of the Linear Model as a supporting tool for climatological studies. In particular, there seems to be promise in the use of the LM in islands like Sardinia that are relatively isolated orographically from other land masses, when the background precipitation is appropriately accounted for.

Acknowledgements

The author would like to thank his supervisor Idar Barstad and co-supervisor Jochen Reuder.

The author would like to thank many friends and colleagues for their helpful advice on this manuscript. The list would be too long to include everyone, but must at least include: Muralidhar Adakudlu, Roohoollah Azad, Jürgen Bader, Knut Barthel, Roberto Deidda, Manuel Losi, Marino Marrocu, Iselin Medhaug, and Justin Wettstein.

I am sure I have forgotten many more.

This research was partially funded by the Bjerknes Center for Climate Research.

References

Anders, A. M., Roe, G. H., Durran, D. R., and Minder, J. R.: Small-Scale Spatial Gradients in Climatological Precipitation on the Olympic Peninsula, Journal of Hydrometeorology, 8, 1068–1081, doi:10.1175/JHM610.1, URL `http://journals.ametsoc.org/doi/pdf/10.1175/JHM610.1`, 2007.

Badas, M. G., Deidda, R., and Piga, E.: Modulation of homogeneous space-time rainfall cascades to account for orographic influences, Natural Hazards and Earth System Sciences, 6, 427–437, 2006.

Banta, R. M.: The role of mountain flows in making clouds, Meteorological Monographs, 23, 229–283, 1990.

Barnes, S. L.: A technique for maximazing details in numerical weather map analysis, Journal of Applied Meteorology, 3, 396–409, 1964.

Barnes, S. L.: Mesoscale objective analysis using weighted timesetime observations. NOAA Tech. Memo. ERL NSSL-62, Tech. rep., National Severe Storms Laboratory, Norman, OK, 1973.

Barstad, I. and Schuller, F.: An extension of Smith's linear theory of orographic precipitation - Introduction of vertical layers, Journal of the Atmospheric Sciences, 68, 2695–2709, 2011.

Barstad, I. and Smith, R. B.: Evaluation of an Orographic Precipitation Model, Journal of Hydrometeorology, 6, 85–99, 2005.

Barstad, I., Grabowski, W. W., and Smolarkiewicz, P. K.: Characteristics of large-scale orographic precipitation, Journal of Hydrology, 340, 78–90, 2007.

Bergeron, T.: The problem of artificial control of rainfall on the globe. Part II, The coastal orographic maxima of precipitation in autumn and winter, Tellus, 1, 15–32, 1949.

Bergeron, T.: Operation and results of "Project Pluvius", in: Physics of Precipitation, Geophysical Monograph, No. 5, pp. 152–157, American Geophysical Union, 1960.

Bergeron, T.: On the low-level redistribution of atmospheric water caused by orography, in: Proceedings of the International Conference on Cloud Physics, May 24 - June 1, 1965: Supplement, pp. 96–100, 1965.

Berry, E. X. and Pranger, M. R.: Equations for calculating the terminal velocities of water drops, Journal of Applied Meteorology, 13, 108–113, 1974.

Bolton, D.: The computation of equivalent potential temperature, Monthly Weather Review, 108, 1046–1053, 1980.

Bond, N. A. and Coauthors: The Coastal Observation and Simulation with Topography (COAST) experiment, Bulletin of the American Meteorological Society, 78, 1941–1955, 1997.

Browning, K. A., Pardoe, C. W., and Hill, F. F.: The nature of orographic rain at wintertime cold fronts, Quarterly Journal of The Royal Meteorological Society, 101, 333–352, 1975.

Bruintjes, R. T., Clark, T. L., and Hall, W. D.: Interactions between topographic airflow and cloud/precipitation development during the passage of a winter storm in Arizona, Journal of the Atmospheric Sciences, 51, 48–67, 1994.

Buzzi, A., N., T., and Malguzzi, P.: Numerical simulations of the 1994 Piedmont flood: Role of orography and moist processes, Monthly Weather Review, 126, 2369–2383, 1998.

Caroletti, G. N. and Barstad, I.: An assessment of future extreme precipitation in western Norway using a linear model, Hydrology and Earth System Sciences, 14, 2329–2341, doi:10.5194/hess-14-2329-2010, 2010.

Chen, Y.-L. and Nash, A. J.: Diurnal variations of surface airflow and rainfall frequencies on the island of Hawaii, Monthly Weather Review, 122, 34–56, 1994.

Christensen, J. H. and Christensen, O. B.: A summary of the PRUDENCE model projections of changes in European climate by the end of this century, Climatic Change, 81, 7–30, doi:10.1007/s10584-006-9210-7, 2007.

Colle, B., Lin, Y., Medina, S., and Smull, B.: Orographic modification of convection and flow kinematics by the Oregon coastal range and Cascades during IMPROVE-2, Monthly Weather Review, 136, 3894–3916, 2008.

Colle, B. A.: Sensitivity of orographic precipitation to changing ambient conditions and terrain geometries: An idealized modeling perspective, Journal of the Atmospheric Sciences, 61, 588–606, 2004.

Colle, B. A., Smith, R. B., and Wesley, D. A.: Mountain Weather Research and Forecasting, chap. Theory, Observations, and Predictions of Orographic Precipitation, pp. 291–344, Springer Atmospheric Sciences, 2013.

Collier, C. G.: A representation of the effects of topography on surface rainfall

within moving baroclinic disturbances, Quarterly Journal of The Royal Meteorological Society, 101, 407–422, doi:10.1256/smsqj.42901, 1975.

Colton, D. E.: Numerical simulation of the orographically induced precipitation distribution for use in hydrological analysis, Journal of Applied Meteorology, 15, 1241–1251, 1976.

Crochet, P., Johannesson, T., Jonsson, T., Sigurdsson, O., Bjornsson, H., Palsson, F., and Barstad, I.: Estimating the Spatial Distribution of Precipitation in Iceland Using a Linear Model of Orographic Precipitation, Journal of Hydrometeorology, 8, 1285–1306, 2007.

Deidda, R.: Multifractal analysis and simulation of rainfall fields in space, Physics and Chemistry of the Earth, 24(1 2), 73–78, 1999.

Deidda, R.: Rainfall downscaling in a space-time multifractal framework, Water Resources Research, 36, 1779–1794, 2000.

Deidda, R., Badas, M., and Piga, E.: Space-time Multifractality of Remotely Sensed Rainfall Fields, Journal of Hydrology, 322, 2–13, doi: 10.1016/j.jhydrol.2005.02.036, 2006.

Déqué, M. and Piedelievre, J. P.: High-Resolution climate simulation over Europe, Climate Dynamics, 11, 321–339, 1995.

Durran, D.: Mountain Waves and Downslope Winds. In Atmospheric Processes over Complex Terrain, Meteorological Monographs, 23, 1990.

Emanuel, K. A.: Atmospheric Convection, Oxford University Press, 1994.

Fraser, A. B., Easter, R. C., and Hobbs, P. V.: A theoretical study of the flow of air and fallout of solid precipitation over mountainous terrain. Part I: Airflow model, Journal of the Atmospheric Sciences, 30, 873–900, 1973.

Galewsky, J. and Sobel, A.: Moist Dynamics and Orographic Precipitation in Northern and Central California during the New Year's Flood of 1997, Monthly Weather Review, 133, 1594–1612, 2005.

Garvert, M. F., Smull, B. F., and Mass, C. F.: Multiscale mountain waves influencing a major orographic precipitation event, Journal of the Atmospheric Sciences, 64, 711–737, 2007.

Giorgi, F. and Mearns, L. O.: Introduction to special section: Regional climate modeling revisited, Journal of Geophysical Research, 104, 6335–6352, 1999.

Gupta, V. K. and Waymire, E. C.: A statistical analysis of mesoscale rainfall as a random cascade, Journal of Applied Meteorology, 32, 251–267, 1993.

Haylock, M. R., Cawley, G. C., Harpham, C., Wilby, R. L., and Goodess, C. M.: Downscaling heavy precipitation over the United Kingdom: a comparison of dynamical and statistical methods and their future scenarios, International Journal of Climatology, 26, 1397–1415, 2006.

Hobbs, P. V., Easter, R. C., and Fraser, A. B.: A theoretical study of the

flow of air and fallout of solid precipitation over mountainous terrain: Part II: Microphysics, Journal of the Atmospheric Sciences, 30, 813–823, 1973.

Hohenegger, C., Brockhaus, P., and Schar, C.: Towards climate simulations at cloud-resolving scales, Meteorologische Zeitschrift, 17, 383–394, 2008.

Houze, R. A., J.: Cloud Dynamics, Academic Press, San Diego, 1993.

Houze, R. A., J.: Orographic effects on precipitating clouds, Reviews of Geophysics, 50, RG1001, doi:10.1029/2011RG000365, 2012.

Hughes, M., Hall, A., and Fovell, R. G.: Blocking in Areas of Complex Topography, and Its Influence on Rainfall, Journal of the Atmospheric Sciences, 66, 508–518, URL http://journals.ametsoc.org/doi/pdf/10.1175/2008JAS2689.1, 2009.

Jarosch, A. H., Anslow, F. S., and Clarke, G. K. C.: High-resolution precipitation and temperature downscaling for glacier models, Climate Dynamics, 38, 391–409, doi:10.1007/s00382-010-0949-1, 2012.

Jiang, Q.: Moist dynamics and orographic precipitation, Tellus, 55A, 301–326, 2003.

Jiang, Q. and Smith, R. B.: Cloud timescales and orographic precipitation, Journal of the Atmospheric Sciences, 60, 1543–1559, 2003.

Koch, S. E., DesJardins, M., and Kocin, P. J.: An interactive Barnes objective map analysis scheme for use with satellite and conventional data, Journal of Climate and Applied Meteorology., 22, 1487–1503, 1983.

Kuo, Y. H. and Chen, G. T. J.: The Taiwan Area Mesoscale Experiment (TAMEX), Bulletin of the American Meteorological Society, 71, 488–503, 1990.

Lenderink, G. and Van Meijgaard, E.: Increase in hourly precipitation extremes beyond expectations from temperature changes, Nature Geoscience, 1, 511–514, 2008.

Lin, Y.-L.: Yearbook of Science & Technology, chap. Dynamics of orographic precipitation, pp. 248–250, McGraw Hill Companies, 2005.

Liston, G. E. and Elder, K.: A Meteorological Distribution System for High-Resolution Terrestrial ModModel (MicroMet), Journal of Hydrometeorology, 7, 217–234, 2006.

Lovejoy, S. and Mandelbrot, B. B.: Fractal properties of rain, and a fractal model, Tellus A, 37A, 209–232, 1985.

Maraun, D., Wetterhall, F., Ireson, A. M., Chandler, R. E., Kendon, E. J., Widmann, M., Brienen, S., Rust, H. W., Sauter, T., Themel, M., Venema, V. K. C., Chun, K. P., Goodess, C. M., Jones, R. G., Onof, C., Vrac, M., and Thiele-Eich, I.: Precipitation downscaling under climate change:

recent developments to bridge the gap between dynamical models and the end user, Reviews of Geophysics, 48, doi:10.1029/2009RG000314, 2010.

Mascaro, G., Vivoni, E. R., and Deidda, R.: Downscaling Soil Moisture in the Southern Great Plains through a Calibrated Multifractal Model for Land Surface Modeling Applications, Water Resources Research, 46, doi: 10.1029/2009WR008855, 2010.

Mascaro, G., Vivoni, E. R., and Deidda, R.: Soil moisture downscaling across climate regions and its emergent properties, Journal of Geophysical Research: Atmospheres, 116, doi:10.1029/2011JD016231, 2011.

Matveev: Fundamentals of General Meteorology - Physics of the Atmosphere, Israel Program for Scientific Translations, 1967.

Meybeck, M., Green, P., and Vorosmarty, C.: A New Typology for Mountains and Other Relief Classes, Mountain Research and Development, 21, 34–45, URL `http://www.jstor.org/stable/3674130`, 2001.

Meyers, M. P. and Steenburgh, W. J.: Mountain Weather Research and Forecasting, chap. Mountain Weather Prediction: Phenomenological Challenges and Forecast Methodology, pp. 1–34, Springer Atmospheric Sciences, 2013.

Miglietta, M. M. and Rotunno, R.: Simulations of moist nearly neutral flow over a ridge, Journal of the Atmospheric Sciences, 62, 1410–1427, 2005.

Miglietta, M. M. and Rotunno, R.: Further results on moist nearly neutral flow over a ridge, Journal of the Atmospheric Sciences, 63, 2881–2897, 2007.

Neiman, P., Ralph, F. M., White, A. B., Kingsmill, D. E., and Persson, P. O. G.: The statistical relationship between upslope flow and rainfall in California's coastal mountains: Observations during CALJET, Monthly Weather Review, 130, 1468–1492, 2002.

Over, T. M. and Gupta, V. K.: Statistical analysis of mesoscale rainfall: Dependence of a random cascade generator on large-scale forcing, Journal of Applied Meteorology, 33, 1526–1542, 1994.

Perica, S. and Foufoula-Georgiou: Model for multiscale disaggregation of spatial rainfall based on coupling meteorological and scaling descriptions, Journal of Geophysical Research: Atmospheres, 101, 26 347–26 361, 1996.

Ralph, F. M., Neiman, P. J., and Rotunno, R.: Dropsonde observations in low-level jets over the northeastern Pacific Ocean from CALJET-1998 and PACJET-2001: Mean Vertical-Profile and Atmospheric-River Characteristics, Monthly Weather Review, 133, 889–910, 2005.

Rasmussen, R., Politovich, M., Marwitz, J., Sand, W., McGinley, J., Smart, J., Pielke, R., Rutledge, S., Wesley, D., Stossmeister, G., Bernstein, B., Elmore, K., Powell, N., Westwater, E., Stankov, B. B., and Burrows, D.:

Winter Icing and Storms Project (WISP), Bulletin of the American Meteorological Society, 73, 951–974, 1992.

Reeves, H. D. and Rotunno, R.: Orographic flow response to variations in upstream humidity, Journal of the Atmospheric Sciences, 65, 3557–3570, 2008.

Reinking, R. F., Snider, J. B., and Coen, J. L.: Influence of storm embedded orographic gravity waves on cloud liquid water and precipitation, Journal of Applied Meteorology, 39, 733–759, 2000.

Reynolds, D. W. and Dennis, A. S.: A Review of the Sierra Cooperative Pilot Project, Bulletin of the American Meteorological Society, 67, 513–523, 1986.

Rhea, J. O.: Orographic precipitation model for hydrometeorological use, Ph.D. thesis, Colorado State University, 1978.

Robichaud, A. J. and Austin, G. L.: On the modelling of warm orographic rain by the seeder-feeder mechanism, Quarterly Journal of The Royal Meteorological Society, 114, 967–988, 1988.

Roe, G.: Orographic Precipitation, Annual Review Of Earth And Planetary Sciences, 33, 645–671, 2005.

Rotunno, R. and Ferretti, R.: Mechanisms of intense alpine rainfall, Journal of the Atmospheric Sciences, 58, 1732–1749, 2001.

Rotunno, R. and Ferretti, R.: Orographic effects on rainfall in MAP cases IOP2b and IOP8, Quarterly Journal of The Royal Meteorological Society, 129, 373–390, 2003.

Rotunno, R. and Houze, Jr., R. A.: Lessons on orographic precipitation from the Mesoscale Alpine Programme, Quarterly Journal of The Royal Meteorological Society, 133, 811–830, 2007.

Rummukainen, M.: Methods of statistical downscaling of GCM simulations, Tech. Rep. 80, Swedish Meteorological and Hydrological Institute, SE-601 76 Norrkoping, Sweden, 1997.

Rummukainen, M.: State-of-the-art with regional climate models, WIREs Clim Change, 1, 82–96, doi:10.1002/wcc.008, 2010.

Salathé Jr., E. P.: Downscaling simulations of future global climate with application to hydrologic modelling, International Journal of Climatology, 25, 419–436, 2005.

Schertzer, D. and Lovejoy, S.: Physical modeling and analysis of rain and clouds by anisotropic scaling of multiplicative processes, Journal of Geophysical Research, 92, 9693–9714, 1987.

Schmidli, J., Goodess, C. M., Frei, C., Haylock, M. R., Hundecha, Y., Ribalaygua, J., and Schmith, T.: Statistical and dynamical downscaling of precipitation: An evaluation and comparison of scenarios for the European Alps, Journal of Geophysical Research, 112, 1–20, 2007.

Schuler, T. V., Crochet, P., Hock, R., Jackson, M., Barstad, I., and Johannesson, T.: Distribution of snow accumulation on the Svartisen ice cap, Norway, assessed by a model of orographic precipitation, Hydrological Processes, 22, 3998–4008, doi:10.1002/hyp.7073, 2008.

Schultz, D. M. and Coauthors: Understanding Utah Winter Storms: The Intermountain Precipitation Experiment, Bulletin of the American Meteorological Society, 83, 189–210, 2002.

Sinclair, M.: A diagnostic model for estimating orographic precipitation, Journal of Applied Meteorology, 33, 1163–1175, 1994.

Smith, R. B.: The influence of mountains on the atmosphere, Advances In Geophysics, 21, 87–230, 1979.

Smith, R. B.: A linear upslope-time-delay model of orographic precipitation, mountain hydrology and water resources, Journal of Hydrology, 282, 2–9, 2003.

Smith, R. B.: Progress on the theory of orographic precipitation, Geological Society of America, Special Paper, 398, 1–16, 2006.

Smith, R. B. and Barstad, I.: A linear theory of orographic precipitation, Journal of the Atmospheric Sciences, 61, 1377–1391, 2004.

Smith, R. B. and Evans, J. P.: Orographic Precipitation and Water Vapor Fractionation over the southern Andes, Journal of Hydrometeorology, 8, 3–19, 2007.

Smith, R. B., Jiang, Q., Fearon, M., Tabary, P., Dorninger, M., and Doyle, J.: Orographic precipitation and air mass transformation: An alpine example, Quarterly Journal of The Royal Meteorological Society, 129, 433–454, 2003.

Smith, R. B., Barstad, I., and Bonneau, L.: The Oregon Climate Transition, Journal of the Atmospheric Sciences, 62, 177–191, 2005.

Stoelinga, M. and Coauthors: Improvement of microphysical parameterization through observational verification experiment, Bulletin of the American Meteorological Society, 84, 1807–1826, 2003.

Storebo, P. B.: Small scale topographic influences on precipitation, Tellus, 28, 45–59, 1976.

Taylor, G. I.: The spectrum of turbulence, Proceedings of the Royal Society A: Mathematical, Physical and Engineering Sciences, 164 (919), 476–490, 1938.

Thornton, P. E., Running, S. W., and White, M. A.: Generating surfaces of daily meteorological variables over large regions of complex terrain, Journal of Hydrology, 190, 214–251, 1997.

Uttal, T., Rauber, R. M., and Grant, L. O.: Distributions of Liquid, Vapor, and Ice in an Orographic Cloud from Field Observations, Journal of the Atmospheric Sciences, 45, 1110–1122, 1988.

Wallace, J. M. and Hobbs, P. V.: Atmospheric Science: An introductory survey, Academic Press (New York), 1977.

Wigley, T. M. L., Jones, P. D., Briffa, K. R., and Smith, G.: Obtaining sub-grid scale information from coarse resolution general circulation model output, Journal of Geophysical Research, 95, 1943–1953, 1990.

Wilby, R. L., Wigley, T. M. L., Conway, D., Jones, P. D., Hewitson, B. C., Main, J., and Wilks, D. S.: Statistical downscaling of general circulation model output: A comparison of methods, Water Resources Research, 34, 1998.

Wratt, D. S., Ridley, R. N., Sinclair, M. R., Larsen, H., Thompson, S. M., Henderson, R., Austin, G. L., Bradley, S. G., Auer, A., Sturman, A. P., Owens, J., Fitzharris, B., Ryan, B. F., and Gayet, J.-F.: The New Zealand Southern Alps Experiment, Bulletin of the Atmospheric Meteorological Society, 77, 683–692, 1996.

Wulfmeyer, V. A., Behrendt, A., Bauer, H.-S., Kottmeier, C., Corsmeier, U., Blyth, A., Craig, G., Schumann, U., Hagen, M., Crewell, S., Di Girolamo, P., Flamant, C., Miller, M., Montani, A., Mobbs, S., Richard, E., Rotach, M. W., Arpagaus, M., Russchenberg, H., Schloessel, P., Koenig, M., Gartner, V., Steinacker, R., Dorninger, M., Turner, D. D., Weckwerth, T., Hense, A., and Simmer, C.: The Convective and Orographic-induced Precipitation Study: A Research and Development Project of the World Weather Research Program for improving quantitative precipitation forecasting in low-mountain regions, Bulletin of the American Meteorological Society, 89, 1477–1486, 2008.

Wurtele, M. G., Sharman, R. D., and Datta, A.: Atmospheric lee waves, Annual Review of Fluid Mechanics, 28, 429–476, 1996.

Xu, C.-Y.: From GCMs to river flow: a review of downscaling methods and hydrologic modelling approaches, Progress in Physical Geography, 23, 229, 1999.

Yau, M. K. and Rogers, R. R.: A Short Course in Cloud Physics, Butterworth-Heinemann, 1989.

Yuter, S. E. and Houze, R. A. J.: Microphysical modes of precipitation growth determined by S-band vertically pointing radar in orographic precipitation during MAP, Quarterly Journal of The Royal Meteorological Society, 129, 455–476, 2003.

Yuter, S. E., Kingsmill, D. E., Nance, L. B., and Loffler-Mang, M.: Observations of Precipitation Size and Fall Speed Characteristics within Coexisting Rain and Wet Snow, Journal of Applied Meteorology and Climatology, 45, 1450–1464, 2006.

List of Tables

III

RMetS
Royal Meteorological Society

Orographic precipitation across an island in southern Norway: model evaluation of time-step precipitation

Idar Barstad[a,b]* and Giulio N. Caroletti[a,c]

[a]*Bjerknes Centre for Climate Research, University of Bergen, Norway*
[b]*UniComputing, UniResearch, Bergen, Norway*
[c]*Università di Cagliari, Dipartimento di Ingegneria Civile, Ambientale e Architettura, Piazza d'Armi, 09123 Cagliari, Italy*

*Correspondence to: I. Barstad, Bjerknes Centre for Climate Research, University of Bergen, Norway.
E-mail: Idar.Barstad@uni.no

Observations of high spatio-temporal resolution from a precipitation network across Stord Island, located off the west coast of southern Norway, are compared to state-of-the-art numerical model simulations. The 12 week long observation period shows a clear orographic precipitation signal across the 10–15 km wide island (peak elevation 750 m). The model experiment designed to capture this signal is run with 9–3–1 km nested grid and results are compared with observations at different accumulation intervals. The total amount of precipitation over the 12 week period is underpredicted, even for the 1 km grid. The maximum precipitation intensity, however, is slightly overpredicted. Time-step (5 s) precipitation from the model is also compared with observed intensities at the highest possible temporal resolution permitted by the rain collection method. The observations indicate that most of the precipitation is formed at intensities from 5 to 20 mm h^{-1}. A smaller fraction of the precipitation is formed with intensities >20 mm h^{-1}. The simulated precipitation at the 3 km grid did not reproduce at the correct intensities. The 1 km grid showed an improved tendency to produce the precipitation at the right intensities, but had too high maximum intensities. A test simulation where the intermediate grid had no cumulus parametrization was performed. Even though effects such as undercatchment and unresolved terrain influenced, it was concluded that the test run performed better than the control run. The investigation concluded that, in general, a 1 km grid is sufficient for capturing the most intensive precipitation event in a satisfying way.

Key Words: time-step precipitation; numerical modelling; high-frequency observations; WRF; Norway; Stord

Received 20 February 2012; Revised 19 September 2012; Accepted 3 October 2012; Published online in Wiley Online Library 27 December 2012

Citation: Barstad I, Caroletti GN. 2013. Orographic precipitation across an island in southern Norway: model evaluation of time-step precipitation. *Q. J. R. Meteorol. Soc.* **139**: 1555–1565. DOI:10.1002/qj.2067

1. Introduction

For sub-daily accumulation periods, impacts due to climate change are closely linked to changes in the probability density function (PDF) of precipitation. The potential effects then depend strongly on the percentile at which the change manifests; a small change in the tail-end of the distribution may have devastating consequences, whereas a relatively large change in the mean will not. Adjustments to new, unaccustomed soil moisture amounts may increase the likelihood of flash floods and landslides (Jaedicke *et al.*, 2008). Situations with an above-normal moisture level in the atmosphere (e.g. transport of subtropical humid air via extratropical cyclones) often result in flooding events (e.g. Lavers *et al.*, 2011). These events are often associated with strong winds forcing air onto mountains, with a

consequent large orographic enhancement of precipitation (e.g. Sodemann *et al.*, 2009) that is often referred to as orographic precipitation (OP). The spatial scale of trigger mechanisms in OP may range from a few hundred metres (small convective cells; e.g. Kirshbaum and Durran, 2005; Kirshbaum and Smith 2009) to a few kilometres (in stably stratified cases; e.g. Smith and Barstad, 2004), scales that are present in most complex terrain formations.

Numerical modelling of atmospheric processes has proven useful in both weather forecasting and in climate assessments. Global climate modelling is somewhat limited by the relatively coarse resolution of both temporal and spatial grids due to available computer resources. This limited resolution has many drawbacks, including the lack of realistic representation of high-intensity precipitation. A possible solution to this problem involves the use of high-resolution limited area models, where the boundaries are supplied by information from a coarse global circulation model (Schmidli *et al.*, 2006; Warner, 2011). This technique is often referred to as *dynamical downscaling* or *regional climate modelling* (RCM). Regional climate modelling provides better resolved terrain, improved parametrization and, to some degree, sharper horizontal and vertical gradients, leading to better resolved extremes (Feser *et al.*, 2011). It is still an open question at what resolution RCMs should be run in order to produce the right level of detail and extremes. The answer depends on the type of assessment. Another open question concerning the RCM utilization is how to apply the lower and lateral boundary conditions deriving from the coupled climate models. Direct use is normally not recommended (Rummukainen, 2010) and some form of adjustment is needed (Barstad *et al.*, 2012), both to surface fluxes and lateral boundary conditions, in order to reproduce the observed atmospheric circulation and related phenomena.

From the more traditional side of precipitation modelling, namely quantitative precipitation forecast (QPF), the literature has increased significantly over the past 10 years. Observational campaigns such as the Mesoscale Alpine Programme (MAP; Binder and Schär, 1996), Improvement of Microphysical Parameterization through Observational Experiment (IMPROVE; Stoelinga *et al.*, 2003) and Convective and Orographically-induced Precipitation Study (COPS; Wulfmeyer *et al.*, 2005) have been the hubs of orographic precipitation research. Recent review articles of Lin *et al.* (2001), Roe (2005), Smith (2006) and Houze (2012) summarize many of these findings. In MAP, the importance of airflow dynamics and stability influenced by latent heat regimes was firmly pointed out (e.g. Jiang, 2003; Colle, 2004). Awareness of the role played by intensification of precipitation due to enhanced cloud liquid water in embedded cellular convective cells is one of the legacies of MAP (e.g. Yuter and Houze, 2003; Kirshbaum and Durran, 2005). The IMPROVE campaigns addressed the microphysical side of OP. For instance, Colle *et al.* (2005) quantified the bulk microphysical processes in a model run of one of the main intensive observational periods. Medina *et al.* (2007) described a model for how the microphysical initiation takes place as a cyclone approaches the terrain; the process commences aloft far upstream and progresses towards the ground as the system moves closer to the foothills. The COPS campaign focused on convective processes in complex terrain, and the goal was to improve the QPF for convective conditions. Results from the campaign led to an improvement of forecasts by water vapour GPS retrieved assimilation, and pointed out the potential impact of biogenic aerosols forming precipitation and that convection in this area is largely driven by advective properties, (Wulfmeyer *et al.*, 2011). The model comparisons showed the windward/lee-side effect associated with convection and a potential fix through increased resolution allowing explicit resolution of convection (Bauer *et al.*, 2011). These campaigns have inspired researchers to develop new, as well as update old, microphysical schemes (e.g. Thompson *et al.*, 2004; Lin and Colle, 2011).

For research based on rain-gauges, the focus has typically been on daily precipitation accumulation intervals, though, in some cases, the temporal resolution is as high as every 3 h. Much less of the research in mountain meteorology has focused on hourly or subhourly accumulation intervals. Radar data studies have by nature focused on the instantaneous picture, which typically isolates to single cases. Intensity duration frequency (IDF) relationships have been studied to a large degree by hydrologists and engineers. These relationships are normally based on distribution fitting of precipitation for different durations, which are then interpolated or fitted through a regression line to obtain the frequency distribution for any duration (e.g. Ceresetti *et al.*, 2010). Other methods to obtain IDFs are also developed: scaling theory (Burlando and Rosso, 1996) and fractal theory (Veneziano *et al.*, 2006).

Our study is motivated by the need to better understand how well current RCM models with state-of-the-art parametrizations are able to simulate precipitation extremes. An increased focus on impacts of climate change and adaptation demands information at ultrahigh frequencies (e.g. 10 min accumulation intervals), as well as high spatial resolution ($\sim$1 km). In this article we seek a better understanding of the model capabilities in handling such ultrahigh frequencies. We pose the following questions. How well do our current numerical models reproduce the spatial and temporal characteristics of high precipitation intensities? Can we gain insight into what is required of models to better resolve these types of precipitation events?

In this article, we compare high-density precipitation observations to fine-scale numerical modelling for a total of 12 weeks over a small, hilly island (Stord) in the coastal zone on the west coast of Norway. The article continues as follows: section 2 is dedicated to explanation and presentation of data and the method, section 3 presents the main results, section 4 contains the discussion and section 5 concludes the article.

2. Data and method

2.1. Observations

The main observational dataset used in this study was acquired in a small field campaign (STOPEX II), which took place in autumn 2006 (26 August to 15 November). The data were recorded across Stord Island, located off the west coast of southern Norway. The island is 10–15 km wide and has mountains 750 m tall (see Figure 1 for geographical information). Reuder *et al.* (2007) presents an overview of the first campaign (STOPEX I) that took place the year prior. The linear theory of Smith and Barstad (2004) produced guidance for the instrumental deployment, and the establishment of the campaign was motivated by the need for detailed precipitation information for evaluation

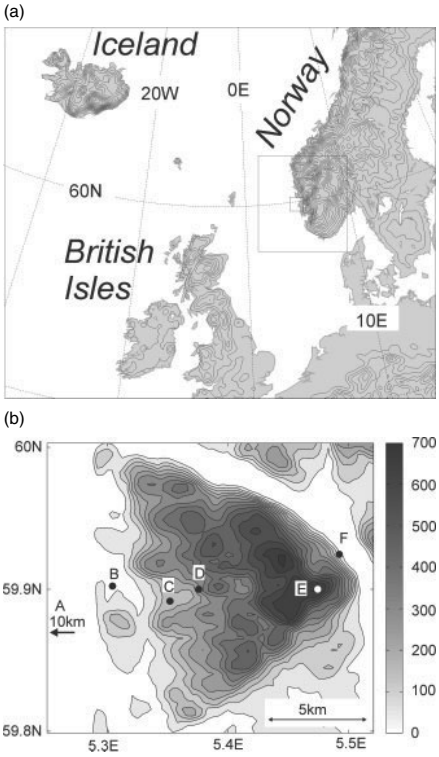

Figure 1. (a) The model domains (9–3–1 km). The terrain for the 9 km grid is shown with contours every 100 m. Land areas are in grey shade. (b) The real terrain (on 90 m grid) of Stord Island contoured every 50 m. Stations are indicated on the plot.

of this theory. See also evaluation of the theory in Barstad and Smith (2005) and simulation results across Stord Island using a two-layer version of the linear theory in Barstad and Schüller (2011).

The second campaign's set-up was a refinement of the first. Eighteen rain-gauges and three weather stations were deployed. Some other instruments were deployed for part of the campaign (microwave rain radar (MRR) and dual GPS data collection). For both campaigns, the set-up and preliminary results are presented in a Master's thesis (Fagerlid, 2007).

Our data are not adjusted for undercatchment, that is, raindrop-enhanced drift past the rain-gauge due to local speed up caused by the collector itself. The deployment for most of the rain-gauges was done in such a way that this problem was minimized; openings in areas of scattered bushes were selected preferentially as gauge placement sites. Above the tree line, weak depressions in the landscape were chosen in order to minimize undercatch. The 'wetting' problem (Michaelides, 2008) was not considered in this report. For the short, 10 min intervals, this may have played some role in the results presented in Table 1. The observation level for the tipping buckets used for rain measurements was 0.2 mm. From the total number of stations, six were selected, see Figure 1(b), and these represent a cross-section of the island. The other stations showed similar signals to those selected. In the discussion we have also used radiosonde data from Sola airport (located 100 km to the south) released routinely every 12 h.

2.2. *Model set-up*

The numerical model used in this study is the Weather Research and Forecasting (WRF) Version 3.3 system. The model's domains with grid spacing of 9–3–1 km applying one-way nesting, is shown in Figure 1. The model top was set to 50 hPa and 70 vertical layers were used. The European Centre for Medium-range Weather Forecasting (ECMWF) analysis was fed to the lateral boundaries every 6 h with sea-surface temperature updates every day. This experiment uses spectral nudging (Miguez-Macho *et al.*, 2004), where waves longer than 1000 km in the analysis were imposed onto the outer nest solution. A 24 h relaxation time was applied. The nudging procedure has proven useful in earlier studies (e.g. Lo *et al.*, 2008) and results in better synchronization with observations and less sensitivity to the location of the lateral boundaries. There was no nudging in the boundary layer. The physical schemes used were: the Kain–Fritsch cumulus scheme (Kain and Fritsch, 1990, 1993; Kain, 2004), the MYJ planetary boundary (PBL) scheme (Mellor and Yamada, 1982; Janjic, 2002) and the microphysics sheme of Thompson *et al.* (2004). The short-wave and long-wave radiation schemes were represented by Dudhia (1989) and the rapid radiative transfer model (RRTM), respectively. See also documentation in Skamarock *et al.* (2005). The convection scheme was turned off for the inner nest. The model time step was set to (45–15–5) s for the three domains. The highest peaks at Stord Island in the 3 and 1 km domains are about 350 m and 550 m, respectively, whereas in reality the highest peaks are 750 m. The choice of using a cumulus scheme in the 3 km grid can be challenged readily, so we tested this by conducting another simulation with the cumulus scheme turned off in the 3 km grid. This is referred to as *nc3km* run, whereas the run previously described is referred to as *the model* or *the control*.

3. Results

At the west coast of Norway, airflow is mainly from a sector spanning from south to west. The water vapour transport shows similar patterns. This is shown for position (60°N, 3°E) in Figure 2. The data are based on a 30 year period (1979–2008) from the ERA-Interim reanalysis (Dee *et al.*, 2011). There are very few cases where the moisture comes from east or northeast and the moisture fluxes are small for these few cases. When comparing the wind rose and the water vapour flux rose, a difference in the maxima can be observed. The more westerly shifted maximum in the water vapour flux, relative to the wind rose, indicates that the zonal component in the wind carries more moisture than the meridional component. This may be due to the general counter-clockwise rotation with height and because the bulk of the moisture is found above the 925 hPa level. We also speculate that terrain shadowing from Scotland to the southwest forces moisture to go around (on the north side of) the Scottish terrain to reach Norway, producing a larger sector to the west in the water vapour rose.

In Figure 3, the vertically integrated horizontal water vapour flux for the 12 week period is shown. It has a clear resemblance to the climatological rose in Figure 2, with a dominating southwesterly moisture flux. The accumulated

Table 1. Rain/no-rain statistics for selected precipitation stations across Stord Island (see Figure 1). Wet events (e.g. '100%' means as observed) and total accumulated amounts in millimetres over the total precipitation period. The numbers are listed as: 'mod (nc3km/**obs**)'. 'Wet' shows in per cent the number of modelled precipitating events over observed events. The 10 min interval is somewhat biased due to the wetting problem with rain-gauges

STOPEX recording stations[a]	Wet (%) 10 min	Wet (%) 1 h	Wet (%) 3 h	Wet (%) 24 h	Total accumulated (mm)
A – Bremnes	92	87	91	102	483 (536/**543**)
B – Korsvik	80	76	83	99	487 (541/**614**)
C – Hovaasen	78	77	86	100	554 (660/**717**)
D – Y-Sorlivatnet	81	82	94	103	693 (808/**838**)
E – Kattnakkjen	68	74	87	97	768 (911/**1239**)
F – Børtveit	79	80	90	102	675 (795/**938**)

[a] From west to east.

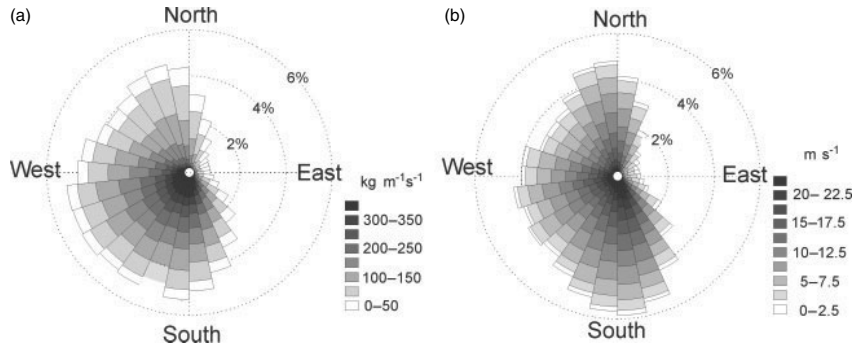

Figure 2. (a)Vertically integrated horizontal water vapour flux (kg m^{-1} s^{-1}) for the period 1979–2008, taken from the ERA-Interim reanalysis valid at (60°N, 3°E). (b) Similar to (a), but for wind speed at 925 hPa.

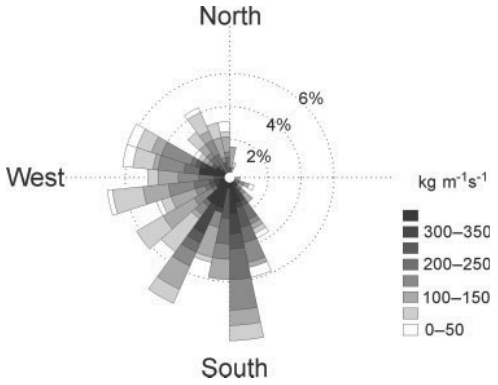

Figure 3. The vertically integrated horizontal water vapour flux for the period investigated (26 August 2006 to 15 November 2006). The data are from the ERA-Interim dataset.

precipitation for the simulation period from 26 August 2006 to 15 November 2006 in the intermediate domain (3 km grid) is shown in Figure 4(a) and (b).

The resolved precipitation dominates the total precipitation field, with the largest values found on the steep slopes along the coastal zone in the middle of western Norway, see Figure 4(a). Convectively parametrized precipitation has a less substantial impact on the total precipitation field, with the largest contributions found in the outer coastal zone and over individual peaks, Figure 4(b). Significant amounts are found out at sea. The picture of the precipitation found in Figure 4(b) fits well with observed values in coastal cross-sections presented by Caroletti and Barstad (2009); the highest values occur in the middle of the coastal zone. They found a larger observed value at the outer coastline than expected from stratiform, orographic precipitation alone. Supported by the precipitation pattern in Figure 4(b), we find it plausible that this is caused by convective activity. Arguably, this is a footprint of the convective available potential energy (CAPE) removal process in the model. The Kain–Fritsch scheme is used for convection in the simulations, and it is a mass flux scheme with low-level control (works through a low-level source layer). It bases its closure on removal of CAPE. The scheme has an explicit, shallow convective part, but this was not turned on during these runs.

Figure 4(c) shows a close up view of the 1 km grid for accumulated precipitation. A clear orographic precipitation signal is evident. The maximum is shifted slightly into the lee side of the Stord Mountains. Farther to the west – over open water – a bubble-like feature can be seen. This feature arises from heavy precipitation on a few occasions in the area. It is natural to attribute this to convective processes as it is detached from terrain. On 28 August 2006, between 1200 and 1800 UTC, such an event took place in the model. For the corresponding period in the observations, a similar tendency occurs: a relatively large increase at the western rain collectors, but with significantly lower values than in the model.

The accumulated precipitation in the 3 km grid for the nc3km run has significantly less total accumulated precipitation (∼20%) than in the control, particularly over the ocean and the coastal zone (not shown). This leaves a larger moisture flux entering the inner domain. Comparing

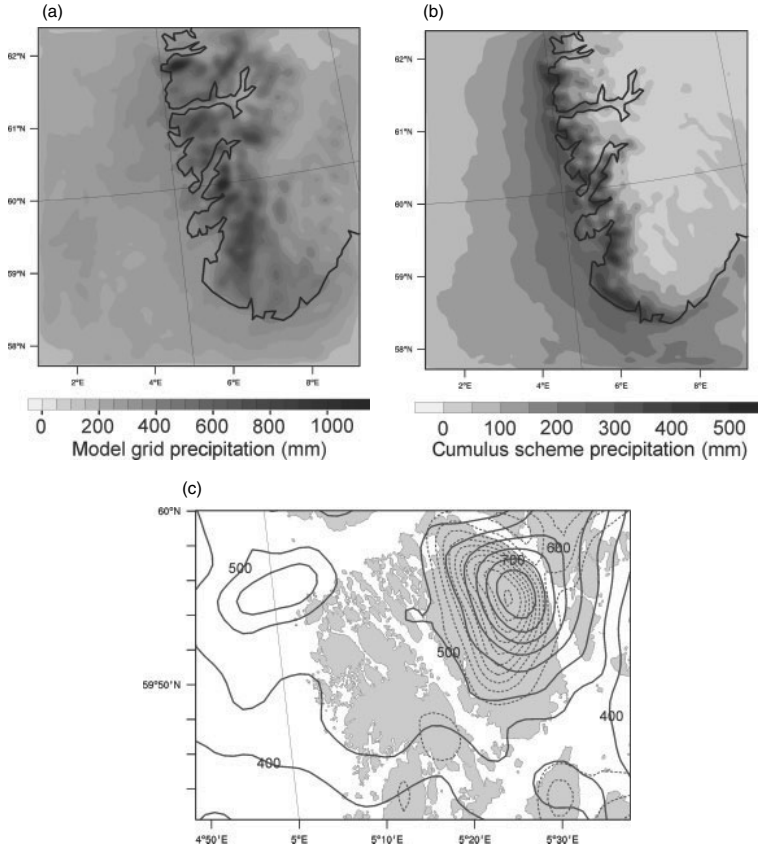

Figure 4. (a) The 3 km domain's resolved accumulated precipitation (mm) for the period. (b) As in (a), but for cumulus scheme precipitation. (c) Total accumulated precipitation across Stord Island with contours every 50 mm (labelled) and terrain contours (broken line) every 50 m, valid for the1 km grid in the control run.

with Figure 4(c) (inner domain), we find the accumulated values for the nc3km run to be significantly higher (∼20%; not shown). The contours of accumulated precipitation are similarly located as in Figure 4(c).

3.1. *Model evaluation*

The rain-gauge data were sampled using tipping buckets, and the model intensities were produced at time-step level taken from the 1 km grid. The data have been arranged so that we compare observations to model data at 10 min, 1 h, 3 h and 24 h accumulation intervals. The surface temperature never dropped below 0°C, so we assume the rain collectors received liquid precipitation only.

We start by evaluating 'rain/no-rain' occurrences (referred to as 'wetness') for selected stations at the west–east cross-section. The data from the stations selected are displayed in Table 1. We also indicate the total accumulated precipitation over the 12 week period for each station (far right column in bold). The nearest-grid-point approach has been used to retrieve values from the model simulations. In order for a fair comparison with the tipping buckets, which have a 0.2 mm threshold for tipping, we move any amounts below this threshold in the model over into next accumulation period. For the 10 min accumulation period, the results show that numbers of wet cases are a bit low. If the 0.2 mm threshold is not used for the model data, the model produces too many rain occurrences (typically 200%–300%). For the longer accumulation periods, the model seems to identify rain and no-rain days reasonably well. The comparison of total precipitation is illuminating; the model produces too little overall precipitation, particularly at the top peak (station E) and in the lee side (station F) of Stord. The run without cumulus parametrization in the 3 km grid (nc3km) shows a better total accumulated precipitation. It also has a slightly higher (about 10%) wetness and thus a better performance (not shown). From this we can conclude preliminarily that the total accumulated precipitation amounts in the model are too small over the island, most probably due to overexcessive drying by the cumulus scheme in the outer domains.

We turn now to precipitation amounts (as opposed to the binary resolved wetness), and start by plotting observed 10 min accumulated values against the simulation for the 1 km domain. In Figure 5(a) we present quantiles from 0.1 to 0.9 represented with lines. In Figure 5(b) we show the highest quantiles (0.95, 0.99 and 0.999) and the maxima for each station. Clearly, the model produces intensities

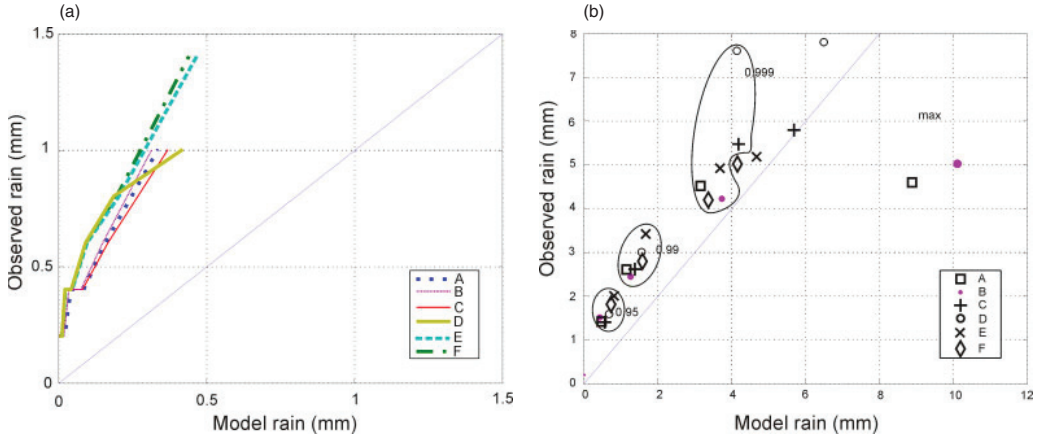

Figure 5. (a) For 10 min accumulation period in the 1 km grid (control simulation): quantile–quantile plot for quantiles from 0.1 to 0.9 and (b) for 0.95, 0.99, 0.999 and maximum. Stations belonging to the same quantile are encircled. This figure is available in colour online at wileyonlinelibrary.com/journal/qj

that are too weak for all levels except the maxima, which are a bit too strong. For Figure 5(b) we see that for the very high level (0.999), the Y-Sørlivatnet (D) station is an outlier. The highest observation value (7.8 mm per 10 min) was measured 1810 UTC on 9 October 2006 and was the peak of a 40 min intense precipitation period, Figure 5(b). Interestingly, this station is situated in the foothills of Stord Island (at about 250 m elevation), the first significant terrain elevation met by an air parcel moving in from the ocean. When comparing maxima values, the model extremes are excessive for A and B (upstream stations on flat land). The maximum values are associated with the strongest convective events and since convection is strongly related to vertical velocities, it is natural to assume that the vertical velocities are too strong in the 1 km grid for these convective cases. We speculate that either diffusion is too weak for updrafts or the buoyancy production at the lower boundary is too strong.

The nc3km run has a similar tendency as shown in Figure 5, but the maxima are more in line with its 0.999 quantile values (not shown). The lower quantiles are similar to those in the control run.

Accumulation periods shorter than 10 min are seldom used for any practical purposes, but we will search for the time-scales in which the precipitation is no longer masked by the length of accumulation interval. We look for the intensities that are most frequent at model time-step resolution. In Figure 6,we show the frequency distribution of model time-step precipitation converted into seconds between bucket tips. For intense precipitation (e.g. a convective character), a narrow peak on the left side is expected. For the less intense (e.g. stratiform character), a peak further to the right is expected.

In Figure 6(a), the observations have the most frequent cases at about 10–15 mm h^{-1} (middle two vertical lines). This level could be interpreted as intermediate-to-strong orographic precipitation – not necessarily including any convection. To the left of the maxima, some stations (upstream, top and lee-side station, which correspond to A, E and F) show a steep dive towards zero, which indicates very few, if any, very high intensity cases (>25 mm h^{-1} (∼29 s between tips)). The stations in between show a further rise, moving toward the zero point on the abscissa, indicating that these stations could benefit from a higher temporal resolution. Using a higher resolution (5 s) for binning, we find all stations to descend towards zero (not shown). When plotting the model simulations of the 1 km and 3 km grid, a different shape appears; for the 1 km grid (Figure 6(b)), a similar skewness to the observations is evident, but the model seems to overestimate the very highest intensities, for the 3 km grid (Figure 6(c)), no clear asymmetric, skewed distribution is seen. The maximum frequency distribution appears at much weaker intensities. In Figure 6(d)–(f), the normalized cumulative frequencies are shown for observations and model results. The impression of the superiority of the 1 km grid manifests itself in these diagrams. The shape of the curves in the 1 km grid are clearly more similar to those observed, Figure 6e. The distance between the lines and the top on the right side of the panels of Figure 6(d)–(f) shows how much emphasis the model has placed on weak intensity events. We see that the model leaves too great a gap, which tells us that too much rain is placed at weak intensities, particularly for the 3 km grid.

Now, inspecting the results from the nc3km run in Figure 6(g)–(j), we find somewhat more agreement between the curve shape of models and observations. The overprediction of maximum values occurring in the 1 km grid are removed and the shapes of the curves are more like those of the observations. Even the 3 km grid has a better shape of the frequency distributions. However, all stations show a deep dive towards zero, also applies stations B and D, which is not supported by the observations. Also, the tops of the frequency distributions are placed too far to the left in the 1 km grid.

From the above, we find that resolving the precipitation intensities at the highest level provides us with new information that would be difficult to gain by evaluating at a 10 min accumulation level. We also see a clear difference between the nc3km run and the control. This is particularly evident looking at the precipitation intensities from the 3 km grid; when a convective scheme is applied, the frequencies distributions of intense precipitation events deteriorate.

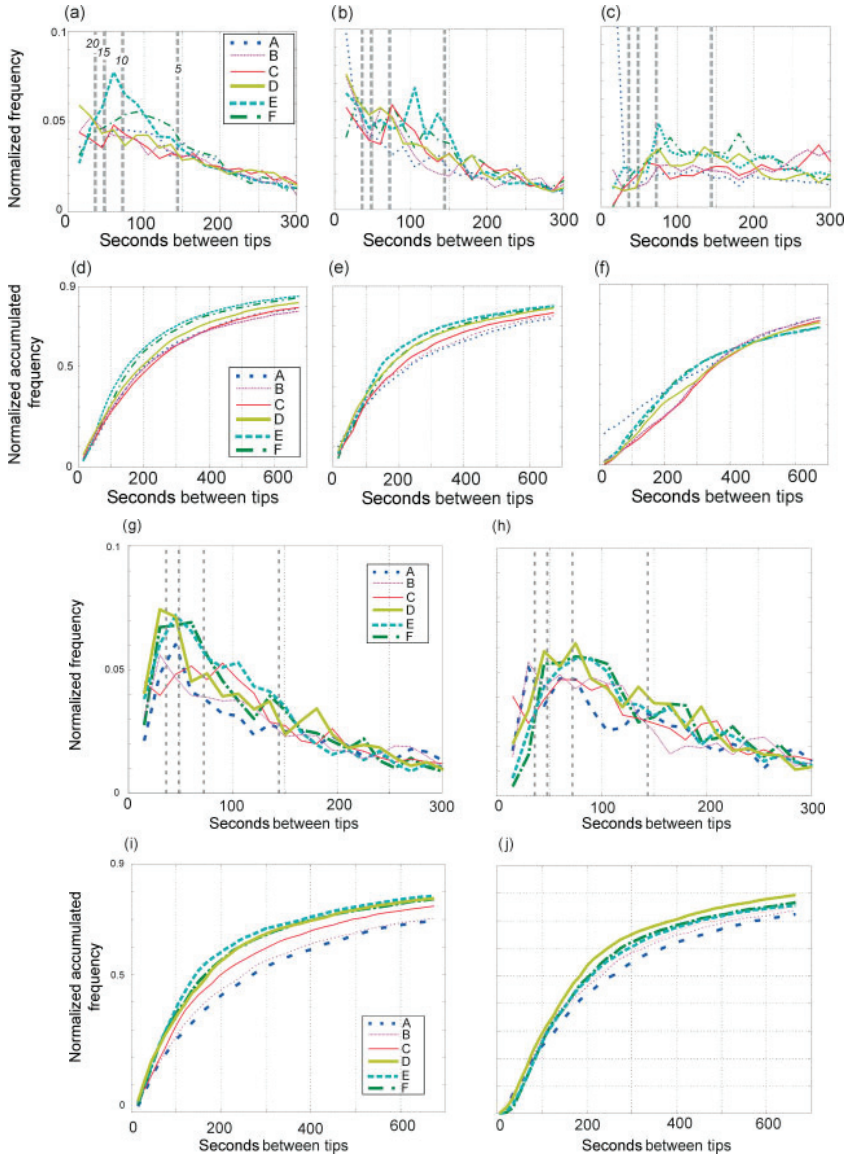

Figure 6. Normalized frequency distribution of bucket tips for (a) observed, (b) 1 km grid, (c) 3 km grid, (g) 1 km grid nc3km run, (h) 3 km grid nc3km run. ((d), (f), (i) and (j)) Similar to above but for cumulative frequency distribution. The abscissa is divided into 15 s intervals (the time step for 3 km grid simulation) so that all datasets can be compared. Broken, grey vertical lines indicate level of intensity as shown in (a) (from right to left: 5, 10, 15 and 20 mm h^{-1}).

Judging from the cumulative frequency plots, we find that all runs have overexcessive drizzle production.

4. Discussion

We have calculated the vertically integrated horizontal moisture flux based on the radiosonde data from Sola airport station for the period of the campaign. In comparison to the model simulation (9 km grid) from the same location, we find the moisture flux to be well simulated for the low flux quantiles (not shown). For higher moisture fluxes, say, above 300 kg m^{-1} s^{-1}, the model flux is too strong (up to about 20%). There are, however, rather few cases above this limit. The difference between the fluxes of the two runs is negligible.

The resolution of terrain has a large impact on vertical velocities and displacements and subsequently precipitation intensities and amounts. When comparing Figure 1(b) and Figure 4(c) we clearly see differences. We tested the precipitation intensity difference between these two terrains using a reduced model (Smith and Barstad, 2004) and discovered that the true terrain (90 m grid) gave about 30%

higher intensities for representative flow conditions. This suggests that the numerical model should underperform in comparison with observed precipitation intensities. The reduced model is, however, designed for stratiform precipitation. Thus the frequent convective rainfall in the coastal mountains may alter this picture substantially.

Undercatchment can be a serious problem particularly in snowy conditions. In our case we have tried to minimize the problem, but we still believe it is affecting the data – particularly at high-elevation stations. We speculate that the effect is in the range of 5–10%.

Taking into consideration the factors mentioned above, the run with parametrized cumulus in the 3 km grid may not be as bad as the first impression. Even though a strict numbers comparison shows an underprediction, the effects mentioned may explain some of the discrepancies. The maximum intensities in the control run, however, are clearly wrong. We judge the effect of the modifying factors mentioned above to be small enough to allow us to suggest that the nc3km run is slightly better with regard to wetness and total accumulation amounts.

For the precipitation produced by forced lifting, properly resolved terrain and gravity waves are important. The vertical velocity profile is controlled by these waves. The waves that penetrate deep into the atmospheric moist layer are properly resolved when the non-hydrostatic effects start to appear. The limit for a stable airflow may be estimated by considering the vertical wave number (e.g. Smith, 2001). For one dimension only, we have:

$$N^2 \sim (Uk)^2 \tag{1}$$

where horizontal wave number is $k = 2\pi/L_x$. Given a characteristic stability of $N = 0.01\ \mathrm{s}^{-1}$ and a wind speed of $U = 10\ \mathrm{m\ s}^{-1}$, we arrive at a length scale, L_x, of about 6 km. A numerical model with grid spacing of 1 km should resolve features with wavelengths of 6–10 km (Skamarock, 2004).

Precipitation produced by convection plays an important role over open water and at the coastal areas. Figure 4(c), left-hand side, shows an example of elevated precipitation amounts over water, due to convection. From Figure 6(b), we have found the high-intensity precipitation (>15 mm/hr) is too frequent in the 1 km grid. We speculate that this is rooted in the model occasionally producing too high vertical velocities in convective cases. This in turn may be related to resolution, organization of shallow convection, and diffusion in the model.

Reuder *et al.* (2007) discussed a record high rain event (measured by daily accumulation) leading to a flooding situation at Stord Island. They found the event to resemble a stratiform precipitation event where the rain shower lasted for several hours. Events of shorter duration, often followed by dry intermittent periods, are frequently observed along the coast. From radar pictures these systems can be attributed to shallow convection organized as open or closed convective cells. These events have the potential to cause local flooding situations of short duration. The convective activity can be ascribed to positive buoyancy produced over a relatively warm ocean and/or from unstable air masses in approaching frontal systems. In any case, this indicates that CAPE and/or potentially unstable conditions ($\mathrm{d}\theta_e/\mathrm{d}z < 0$, where θ_e is the equivalent potential temperature) are present. Evidently, the presence of convection has a significant impact on the precipitation patterns, cf. Figure 4(b).

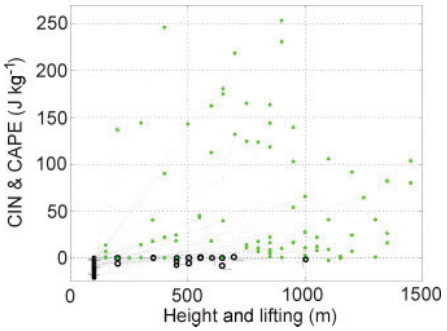

Figure 7. Information from radiosondes (12 h) at the nearby Sola airport during STOPEX II (14% of the 17% missing data were completed by data from the Ekofisk sonde). One event has both a dot and a circle and is linked by a thin, broken line. Dots: Amount of convective available potential energy (CAPE; *y*-axis) and lifting (*x*-axis) needed for realization of the CAPE potential (only cases between 0 and 1500 m are shown). Circles: convective inhibition (CIN; *y*-axis) which has to be overcome before release of CAPE. The height at which the CI -layer starts is shown by the *x*-position of the circles. The CAPE is calculated by lifting the warmest parcels (adiabatically adjusted) residing in the lowest 500 m up to 5 km altitude. This figure is available in colour online at wileyonlinelibrary.com/journal/qj

In the cumulus parametrization scheme, CAPE plays an important role, and this makes it natural to have a closer look into the CAPE conditions during the campaign. Potential instability is difficult to quantify as it depends on which vertical layer the lifting takes place. We have investigated the CAPE of air approaching Stord Island during the campaign. At Sola airport, 100 km south of Stord Island, radiosondes are released routinely every 12 h. For this campaign, the Sola station had about 83% coverage, and the missing data have been completed to 97% by the radiosonde launches from the Ekofisk oil platform (about 300 km to the south-southwest). By using this sonde information, we have mapped the CAPE versus the lifting needed to release the CAPE. This is shown in Figure 7.

The results from the radiosonde data shown in Figure 7 indicate that 66% of the cases will release CAPE if enough lifting is provided. The mountains of southern Norway are roughly 1500 m in elevation, and by lifting to this level, 52% of the cases will potentially release CAPE. Averaged over the lower 1 km (chosen somewhat arbitrarily), about 59% of the cases indicate potential instability ($\mathrm{d}\theta_e/\mathrm{d}z < 0$) (not shown). The CAPE and potential instability appeared at the same time in 42% of the cases. It is reasonable to assume that air moving up the foothills of western Norway will trigger convection. The lifting produced by the mountains starts far upstream (∼100 km; e.g. Barstad and Grønås, 2005), and the extent of the lifting is given by the deformation length-scale, *Nh/f* (Pierrehumbert and Wyman, 1985). This can explain why the convective scheme was triggered over open ocean as seen in Figure 4.

In order to relate upstream ambient conditions to extreme precipitation, we will now identify the cases exceeding the 0.99 quantile (q99) for the 10 min accumulation intensity. Figure 8 shows the scatter plots with CAPE, convective inhibition (CIN) and the condition for potential instability ($\mathrm{d}\theta_e/\mathrm{d}z < 0$), wind speed and surface temperature for the 31 radiosondes ascribed to rain-gauges, which on average have one or more exceeding the q99 level.

In Figure 8(b) we find 10 cases with CAPE values above $100\ \mathrm{J\,kg}^{-1}$. The associated wind speeds are relatively low (less

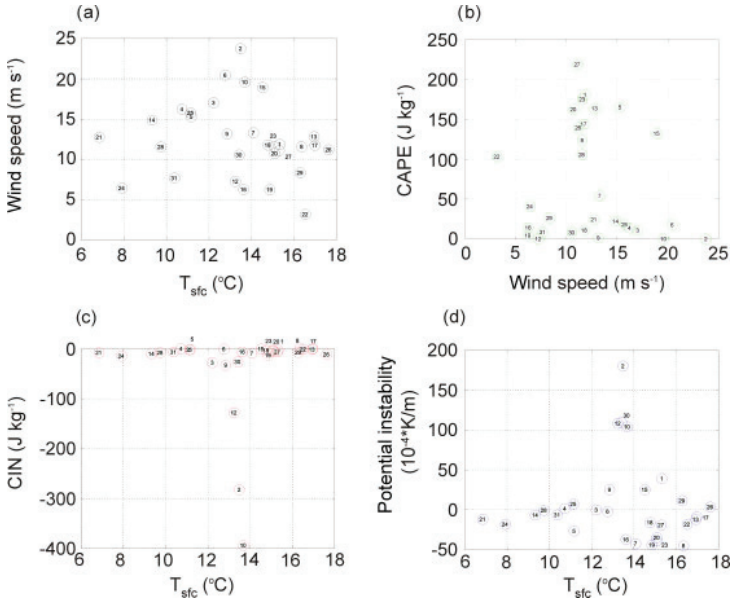

Figure 8. Information from radiosondes for the campaign period associated with the highest (q99) 10 min accumulation intensities for stations across the traverse. (a) Wind speed (averaged between 250–500 m) versus surface temperature (° C); (b) CAPE versus wind speed; (c) CIN versus surface temperature; (d) $d\theta_e/dz \times 10^4$ versus surface temperature where negative values indicate unstable cases. All 31 cases exceeding the q99 level are indicated by rank. This figure is available in colour online at wileyonlinelibrary.com/journal/qj

than 13 m s^{-1}). Two other high CAPE cases in Figure 8(b) are associated with high wind speeds (cases 5 and 15). Two cases with low CIN value (cases 2 and 10) are linked directly to high winds and large values for the potential instability indicator. One of these cases (case 2) is also the case with highest winds (24 m s^{-1}). In Figure 8(a), where we focus on the average wind speed in the lower PBL versus surface temperature, we see that the temperature has to be above 10–12°C before we can expect extremes. Likewise for the wind speed, most extremes seem to be associated with winds above 8 m s^{-1}. In Figure 8(a) we see that, except for case 25, the strongest extreme cases are associated with strong winds.

A relatively warm sea will build up the convective capacity – both through CAPE but also through moisture and potential instability. Advection toward the coastal mountains, where a general broad lifting starts, will intensify the precipitation in the coastal zone. After moving past the first lifting area near the coastal mountains, the air will lose most of its convective potential, and more regular orographic precipitation is then expected farther inland. In cases where a convection scheme depletes the air of moisture and CAPE, reduced precipitation must be expected. Convective schemes seem to be overenthusiastic in this regard, which is referred to as the 'windward–lee effect'. See, among others, Schwitalla *et al.* (2008). We have compared the averaged and the quantiles of the vertically integrated horizontal water vapour flux in the 1 km grid, and found the flux to be very similar for the two runs. This indicates that depletion of buoyancy is most likely the cause of the difference, not the moisture.

Our findings based on radiosonde information have to be considered cautiously; the 12 h radiosondes information is rather coarse in comparison to the 10 min accumulated precipitation. Sharp fronts separating varying air masses passing rapidly through the area will potentially make the radiosonde information unrepresentative of the rain observational area.

The CAPE concept does not fully explain the convective activity (Stevens, 2005). The convection due to potential instability is difficult to measure. In shallow convective systems with many individual cells, a compensating downward motion is warranted in between the convective updrafts. The cloud fraction area plays a decisive role (Kirshbaum and Smith, 2009).

5. Conclusion

This article has presented precipitation from a model run with a 9–3–1 km grid compared with observations from a 12 week campaign conducted in autumn 2008. Rain-gauges with high temporal resolution were deployed across the small island Stord at the western coast of Norway. A clear orographic precipitation signal was observed and model results with time-step resolution were compared.

The model suggests a significant convective precipitation component, particularly over the sea and over the coastal mountains. On daily accumulation intervals, the model performs well in reproducing the number of rain occurrences. For sub-daily accumulation periods (10 min, 1 h and 3 h), the model underpredicts the number of rain occurrences (70–90% of total). However, from model time-step investigations we have reason to believe that the model produces too much drizzle. The underprediction of rain occurrences thus comes from the threshold introduced in order for a fair comparison with the tipping buckets. When evaluating the amounts of total precipitation for the campaign, we find that the model underpredicts and simulates only 60–90% of the observed totals. Taking into consideration effects not

included in the model such as full terrain resolution and possible undercatchment of rain-gauges, the general results are slightly improved. However, the discrepancy cannot be fully explained. The study also includes observational comparison of precipitation intensities on model time-step level. The results show that increased horizontal resolution (to 1 km grid spacing) improves the time-step precipitation intensities in comparison with the 3 km grid. Except for the highest precipitation intensities, the shape of the frequency distributions in the 1 km grid seems more like the observed than in the 3 km grid.

A test run where convection was allowed to form without parametrization in the intermediate 3 km grid shows that the representation of convection plays a significant role both for the intensities and for the total accumulated precipitation. The total accumulated precipitation and the wetness clearly show an improvement.

Extreme precipitation events were investigated. Radiosonde data show that 66% of the cases had potential of releasing CAPE, and the presence of CAPE increases the likelihood of extreme precipitation intensities. On the other hand, extremes may also exist without significant amounts of CAPE, but would then require stronger winds.

This article has shown that the total accumulated precipitation compiled out of events with moderate to intense precipitation (>5 mm h^{-1}), with accumulation levels as short as 10 min, does not necessarily reveal the whole picture. Model time-step intensities may be important for assessment of flash-flood situations, and design of future observational campaigns should keep this in mind. We find that the 1 km grid spacing can, to a large degree, do a satisfying job simulating these kinds of problems. For some applications requiring information of very high intensities, a 3 km grid may not be good enough.

Acknowledgements

Discussions with S. P. Sobolowski and A. Sorteberg are greatly appreciated. The authors appreciate assistance from Melissa Wrzesien and two anonymous reviewers in improving the manuscript.

References

Barstad I, Grønås S. 2005. Southwesterly flows over southern Norway – mesoscale sensitivity to large-scale wind direction and speed. *Tellus* **57A**: 136–152.

Barstad I, Schüller F. 2011. An extension of Smith's linear theory of orographic precipitation – introduction of vertical layers. *J. Atmos. Sci.* **68**: 2695–2709.

Barstad I, Smith RB. 2005. Evaluation of an orographic precipitation model. *J. Hydrometeorol.* **6**: 85–99.

Barstad I, dos Mesquita M, Sorteberg I. 2012. Present and future offshore wind power potential in northern Europe based on downscaled global climate runs with adjusted SST and sea ice cover. *Renewable Energy*. DOI: 10.1016/j.renene.2012.02.008.

Bauer H-S, Weusthoff T, Dorninger M, Wulfmeyer V, Schwitalla T, Gorgas T, Arpagaus M, Warrach-Sagi K. 2011. Predictive skill of a subset of models participating in D-PHASE in the COPS region. *Q. J. R. Meteorol. Soc.* **137**: 287–305.

Binder P, Schär C (eds). 1996. *MAP – Mesoscale Alpine Programme Design Proposal*. MAP Programme Office; 77 pp. [Available from Swiss Meteorological Institutte, Krähbühlstrasse 58, CH-8044 Zürich, Switzerland.]

Burlando P, Rosso R. 1996. Scaling and multiscaling depth–duration–frequency of storm precipitation. *J. Hydrol.* **187**(1–2): 45–64.

Caroletti GN, Barstad I. 2010. An assessment of future extreme precipitation in western Norway using a linear model. *Hydrol. Earth Syst. Sci.* **14**: 2329–2341.

Ceresetti D, Molinié G, Creutin J-D. 2010. Scaling properties of heavy rainfall at short duration: A regional analysis. *Water Resour. Res.* **46**: W09531. DOI: 10.1029/2009WR008603.

Colle BA. 2004. Sensitivity of orographic precipitation to changing ambient conditions and terrain geometries: An idealized model perspective. *J. Atmos. Sci.* **61**: 588–606.

Dee DP, Uppala SM, Simmons AJ, Berrisford P, Poli P, Kobayashi S, Andrae U, Balmaseda MA, Balsamo G, Bauer P, Bechtold P, Beljaars ACM, van de Berg L, Bidlot J, Bormann N, Delsol C, Dragani R, Fuentes M, Geer AJ, Haimberger L, Healy SB, Hersbach H, Holm EV, Isaksen L, Kallberg P, Köhler M, Matricardi M, McNally AP, Monge-Sanz BM, Morcrette J-J, Park B-K, Peubey C, de Rosnay P, Tavolato C, Thépaut J-N, Vitart F. 2011. The ERA-Interim reanalysis: configuration and performance of the data assimilation system. *Q. J R. Meteorol Soc.* **137**: 553–597.

Dudhia J. 1989. Numerical study of convection observed during the winter monsoon experiment using a mesoscale two-dimensional model. *J. Atmos. Sci.* **46**: 3077–3107.

Fagerlid GO. 2007. *Small scale orographic precipitation: A study of phase I and II of the STord Orographic Precipitation Experiment (STOPEX)*. Master thesis, Geophysical Institute, University of Bergen, Norway; 103 pp.

Feser F, Rockel B, Storch Hv, Winterfeldt J, Zahn M. 2011. Regional climate models add value to global model data. *Bull. Am. Meterol. Soc.* **92**: 1181–1192.

Houze RA Jr. 2012. Orographic effects on precipitating clouds. *Rev. Geophys.* **50**: RG1001. DOI: 10.1029/2011RG000365.

Janjic ZI. 2002. *Nonsingular Implementation of the Mellor-Yamada Level 2.5 Scheme in the NCEP Meso Model*. Office Note No. 437, National Centers for Environmental Prediction: College Park, MD; 61 pp.

Jaedicke C, Solheim A, Blikra LH, Sorteberg A, Aasheim A, Kronholm K, Vikhamar-Schuler D, Isaksen K, Sletten K, Kristensen K, Barstad I, Melchiorre C, Høydal ØA, Mestl H. 2008. Spatial and temporal variations of Norwegian geohazards in a changing climate, the GeoExtreme Project. *Nat. Hazards Earth Syst. Sci.* **8**: 893–904.

Jiang Q. 2003. Moist dynamics and orographic precipitation. *Tellus A* **55**: 301–316.

Kain JS. 2004. The Kain–Fritsch convective parameterization: An update. *J. Appl. Meteorol.* **43**: 170–181.

Kain JS, Fritsch JM. 1990. A one-dimensional entraining/detraining plume model and its application in convective parameterization. *J. Atmos. Sci.* **47**: 2784–2802.

Kain JS, Fritsch JM. 1993. Convective parameterization for mesoscale models: The Kain–Fritcsh scheme. In: *The Representation of Cumulus Convection in Numerical Models*, Emanuel KA, Raymond DJ (eds). American Meteorological Society; 246 pp.

Kirshbaum DJ, Durran DR. 2005. Factors governing cellular convection in orographic precipitation. *J. Atmos. Sci.* **61**: 682–698.

Kirshbaum DJ, Smith RB. 2009. Orographic precipitation in the Tropics: Large-eddy simulations and theory. *J. Atmos. Sci.* **66**: 2559–2578.

Lavers DA, Allan RP, Wood EF, Villarini G, Brayshaw DJ, Wade AJ. 2011. Winter floods in Britain are connected to atmospheric rivers. *Geophys. Res. Lett.* **38**: L23803, 1–8.

Lin Y-L, Colle BA. 2011. A new microphysical scheme that includes riming intensity and temperature-dependent ice characteristics. *Mon. Weath. Rev.* **139**: 1013–1035.

Lin Y-L, Chiao S, Wang T-A, Kaplan ML, Weglarz RP. 2001. Some common ingredients for heavy orographic rainfall. *Weath. Forecast.* **16**: 633–660.

Lo JC-F, Yang Z-L and Pielke RA Sr. 2008. Assessment of three dynamical climate downscaling methods using the Weather Reasearch Forecasing (WRF) model. *J. Geophys. Research*, **113**: 1–16, DOI: 10.1029/2007JD009216.

Medina S, Sukovich E, Houze RA Jr. 2007. Vertical structures of precipitation in cyclones crossing the Oregon cascades. *Mon. Wea. Rev.* **135**: 3565–3586.

Mellor GL, Yamada T. 1982. Development of a turbulence closure model for geophysical fluid problems. *Rev. Geophys.* **20**: 851–875.

Miguez-Macho G, Stenchikov G, Robock A. 2004. Spectral nudging to eliminate the effects of domain position and geometry in regional climate model simulations. *J Geophys Res* **109**: D13104. DOI: 10.1029/2003JD004495.

Michaelides, S. (Ed.) 2008. *Precipitation: Advances in Measurement, Estimation and Prediction*. Springer-Verlag; 540 pp.

Pierrehumbert R, Wyman B. 1985. Upstream effects of mesoscale mountains. *J. Atmos. Sci.* **42**: 977–1003.

Reuder J, Barstad I, Fargerlid GO, Sandvik AD. 2007. Stord Orographic Precipitation Experiment (STOPEX): An overview of phase I. *Hydrol. Earth Syst. Sci.* **10**: 17–23.

Roe GH. 2005. Orographic precipitation. *Ann. Rev. Earth Planet. Sci.* **33**: 645–671.

Rummukainen M. 2010. State-of-the-art with regional climate models. *Rev. Clim. Change* **1**: 82–96. DOI: 10.1002/wcc.008

Skamarock WC. 2004. Evaluating mesoscale NWP models using kinetic energy spectra. *Mon. Wea. Rev.* **132**: 3019–3032.

Skamarock WC, Klemp JB, Dudhia J, Gill DO, Barker DM, Wang W, Powers JG. 2005. *A Description of the Advanced Research WRF Version 2*. Tech Notes-468+STR, National Center for Atmospheric Research: Boulder, CO.

Schmidli J, Frei C, Vidale PL. 2006. Downscaling from GCM precipitation: a benchmark for dynamical and statistical downscaling methods. *Int. J. Climatol.* **26**: 679–689.

Schwitalla T, Zängl G, Bauer H-S, Wulfmeyer V. 2008. Systematic errors of QPF in low-mountain regions. *Special Issue on Quantitative Precipitation Forecasting. Meteorol. Z.* **17**: 903–919. DOI: 10.1127/0941-2948/2008/0338.

Smith RB. 2001. Stratified flow over topography. In *Environmental Stratified Flows*, Grimshaw R (ed.). Kluwer Academic Publisher; 284 pp.

Smith RB. 2006. Progress on the theory of orographic precipitation. In *Special Paper 398: Tectonics, Climate, and Landscape Evolution*, Willett SD, Hovius N, Brandon M, Fisher D (eds). Geological Society of America: Boulder, CO.

Smith RB, Barstad I. 2004. A linear theory of orographic precipitation. *J. Atmos. Sci.* **61**: 1377–1391.

Sodemann H, Wernli H, Schwierz C. 2009. Sources of water vapour contributing to the Elbe flood in August 2002 – A tagging study in a mesoscale model. *Q. J. R. Meteorol. Soc.* **135**: 205–223.

Stevens B. 2005. Atmospheric moist convection. *Ann. Rev. Earth Planet Sci.* **33**: 605–643.

Stoelinga MT, Hobbs PV, Mass CF, Locatelli JD, Bond NA, Colle BA, Houze Jr RA, Rango A. 2003. Improvement of microphysical parameterization through observational verification experiment (IMPROVE). *Bull. Am. Meteorol. Soc.* **84**: 1807–1826.

Thompson G, Rasmussen RM, Manning K. 2004. Explicit forecasts of winter precipitation using an improved bulk microphysics scheme. Part I: Description and sensitivity analysis. *Mon. Weath. Rev.* **132**: 519–542.

Veneziano D, Langousis A, Furcolo P. 2006. Multifractality and rainfall extremes: A Review. *Wat. Resour. Res.* **42**: W06D15. DOI: 10.1029/2005WR004716.

Warner TT. 2011. *Numerical Weather and Climate Prediction*. Cambridge University Press; 526 pp.

Wulfmeyer V, Behrendt A, Kottmeier C, Corsmeier U (eds). 2005. *COPS Science Overview Document*. Available from http//:www.uni-hohenheim.de/cops

Wulfmeyer V, Behrendt A, Kottmeir C, Corsmeier U, Barthlott C, Craig GC, Hagen M, Althausen D, Aoshima F, Arpagaus M, Bauer HS, Bennett L, Blyth A, Brandau C, Champollion C, Crewell S, Dick G, di Girolamo P, Dorninger M, Dufournet Y, Eigenmann R, Engelmann R, Flamant C, Foken T, Gorgas T, Grzeschik M, Handwerker J, Hauck C, Holler H, Junkermann W, Kalthoff N, Kiemle C, Klink S, Konig M, Krauss L, Long CN, Madonna F, Mobbs S, Neininger B, Pal S, Peters G, Pigeon G, Richard E, Rotach MW, Russchenberg H, Schwitalla T, Smith V, Steinacker R, Trentman J, Turner DD, van Baelen J, Vogt S, Volkert H, Weckwerth T, Wernli H, Wieser A, Wirth M. 2011. The Convective and Orographically-induced Precipitation Study (COPS): the scientific strategy, the field phase, and research highlights. *Q.J.R. Meteorol. Soc.* **137**: 3–30.

Yuter SE, Houze RA. 2003. Microphysical modes of precipitation growth determined by S-band vertically pointing radar in orographic precipitation during MAP. *Q.J.R. Meteorol. Soc.* **129**: 455–476.

